UNIVERSIDADE DE LISBOA

FACULDADE DE MEDICINA

Neuromuscular transmission modulation by A_{2A} adenosine receptors in the SOD1G93A mouse model of Amyotrophic Lateral Sclerosis

Filipe Jorge do Nascimento Xavier Fernandes

Curso de Mestrado em Neurociências

Lisboa, 2013

UNIVERSIDADE DE LISBOA

FACULDADE DE MEDICINA

Neuromuscular transmission modulation by A_{2A} adenosine receptors in the SOD1G93A mouse model of Amyotrophic Lateral Sclerosis

Filipe Jorge do Nascimento Xavier Fernandes

Orientador: Professor Doutor Joaquim. A. Ribeiro
Faculdade de Medicina de Lisboa e Instituto de Medicina Molecular

Co-Orientador: Doutora Alexandra M. Correia
Museu Nacional de História Natural e da Ciência e Instituto de Medicina Molecular

Curso de Mestrado em Neurociências

Lisboa, 2013

Esta dissertação foi aprovada pelo Conselho Científico da Faculdade de Medicina da Universidade de Lisboa em reunião de 15 de Outubro de 2013

Index

Abstract

Amyotrophic Lateral Sclerosis (ALS) is an adult-onset progressive neurodegenerative disease characterized by the selective loss of motor neuron function leading to muscle atrophy and weakness. After symptoms onset patients last 4 to 5 years and ultimately die due to bulbar failure.

Animal models have been developed to study the neurobiology of ALS, with the SOD1G93A mouse model as the most studied so far. Morphological and functional abnormalities have been reported in both pre-symptomatic and symptomatic stages of ALS progression in this rodent model. Dysfunctions in neuromuscular transmission at phrenic nerve-hemidiaphragm preparations of the SOD1G93A mouse have recently been put in evidence by our group. Since adenosine A_{2A} receptors (A2AR) play a major role in fine-tuning neurotransmitter release in mammalian neuromuscular junctions (NMJs), we decided to evaluate how A2AR modulate acetylcholine (ACh) release in pre-symptomatic (4-6 weeks old (wo)) and symptomatic (12-14 wo) SOD1G93A mice.

Using the selective A2AR agonist CGS 21680, we performed a dose-response study using 3, 5 and 10 nM in pre-symptomatic SOD1G93A mice and age-matched Wild Type (WT) animals. CGS 21680 at 3, 5, 10 and 25 nM was studied in symptomatic SOD1G93A and 12-14 wo WT rodents. 25 nM was used in the previous mentioned group of animals to verify if at concentrations higher than 10nM CGS 21680 effect in NMT would be increased. Intracellular recordings of endplate potentials (EPPs), miniature endplate potentials (MEPPs) and giant miniature endplate potentials (GMEPPs) where performed in

high [Mg^{2+}] paralyzed phrenic nerve-hemidiaphragm preparations. Low-frequency stimuli (0.5 Hz) allowed the evaluation of the evoked activity (EPPs) while spontaneous activity (MEPPs and GMEPPs) was measured in gap-free intervals. *Quantal content* (QC) was measured as the ratio between the mean EPP amplitude and the mean MEPP amplitude recorded in the same period of time.

We first validated high [Mg^{2+}] as an useful method to study neuromuscular transmission (NMT) in these mice. The shift in the Ca^{2+}/Mg^{2+} ratio preserved the previous described features of ACh release in SOD1G93A mice diaphragm fibers.

In the pre-symptomatic phase, SOD1G93A mice displayed a significant increase in EPP amplitude and QC in tested concentrations of CGS 21680 when compared to WT mice ($p<0.05$ Unpaired *t*-test) except for EPP changes at 3nM ($p>0.05$ Unpaired *t*-test). MEPP and GMEPP amplitude were not changed by CGS 21680 ($p>0.05$ Paired *t*-test). The A2AR-mediated increase in MEPP frequency was not statistically different between both groups in the presence of 3 and 10nM of the A2AR agonist ($p>0.05$ Unpaired *t*-test), but was significantly higher in SOD1G93A mice when perfused at 5nM ($p<0.05$ Unpaired *t*-test). We also found that in the pre-symptomatic SOD1G93A fibers GMEPP frequency was statistically higher in the presence of CGS 21680 (5nM) than in age-matched WT NMJs ($p<0.05$ Unpaired *t*-test).

In the symptomatic phase, CGS 21680 did not elicit any changes in SOD1G93A mice evoked (EPP amplitude and QC) and spontaneous (MEPP and GMEPP frequency and amplitude) activity from SOD1G93A mice ($p>0.05$

Paired *t*-test). When 0.5 Hz stimuli were delivered, EPP amplitude, QC and MEPP frequency were increased in 12-14 wo WT mice in the presence of 3, 5, 10 and 25 nM of CGS 21680 ($p<0.05$ Paired *t*-test). These parameters together with GMEPP frequency were significantly higher than in symptomatic mice ($p<0.05$ Unpaired *t*-test). GMEPP and MEPP amplitude were not changed by CGS 21680 in older WT mice ($p>0.05$ Paired *t*-test).

The A2AR receptor antagonist SCH 58261 (50nM) was devoid of effect in spontaneous and evoked release ($p>0.05$ Paired t-test) and effectively blocked CGS 21680 (5nM in 4-6 wo mice and 10 nM in 12-14 wo WT rodents) facilitation ($p<0.05$ one-way ANOVA followed by Tukey's pos-hoc).

Our results strongly suggest an early functionally enhancement of NMT concerning adenosine modulation before symptoms appear. This dysfunction involves an A2AR functional upregulation at diaphragm NMJs in pre-symptomatic SOD1G93A mice.

When symptoms start to develop, A2AR receptor function is lost in symptomatic SOD1G93A mice but remains present in 12-14 wo WT mice. Furthermore, CGS 21680 perfusion triggered a higher A2AR facilitation in 12-14 wo than in 4-6 wo WT mice. This might be attributable to a normal maturation feature of the studied synapse, which contrasted with the observations in transgenic mice.

The shift from a functional upregulation of A2AR before symptomatology that arises in SOD1G93A mice towards an apparent loss of A2AR functionality in symptomatic phase, highlights the role of this subtype of P1 receptors in the

scope of ALS. A2AR targeted drugs could eventually play an import role in the delay of this disease.

Resumo

A Esclerose Lateral Amiotrófica (ALS) é uma doença neurodegenerativa progressiva caracterizada pela perda seletiva da função do neurónio motor, levando a atrofia e fraqueza muscular. Após o início dos sintomas a esperança de vida dos doentes é de cerca de 4 a 5 anos, sendo a causa da morte geralmente devida a insuficiência respiratória.

Modelos animais têm sido desenvolvidos para estudar a neurobiologia da ALS, sendo o do murganho SOD1G93A o mais estudado. Neste modelo, anormalidades morfológicas e funcionais têm sido relatadas em ambos os estadios pré-sintomático e sintomático da ALS. Disfunções na transmissão neuromuscular (NMT) em preparações de nervo frénico-hemidiafragma de murganho SOD1G93A foram recentemente postas em evidência pelo nosso grupo. Considerando que os recetores A_{2A} de adenosina (A2AR) desempenham um papel importante no controlo da libertação de acetilcolina (ACh) na junção neuromuscular (NMJ) de mamífero, explorámos o papel dos A2AR na modulação da NMT em murganhos SOD1G93A nas fases pré-sintomática (4-6 semanas de idade) e sintomática (12-14 semanas de idade).

Usando o agonista seletivo dos A2AR (CGS 21680), foi realizado um estudo de dose-resposta utilizando concentrações de 3, 5 e 10 nM em animais pré-sintomáticos SOD1G93A e *Wild Type* (WT) (4-6 semanas). CGS 21680 a 3, 5, 10 e 25 nM foi utilizado em murganhos sintomáticos SOD1G93A e WT (12 - 14 semanas). A concentração 25 nM foi testada neste último grupo, de modo a verificar se a concentrações superiores a 10 nM o efeito modulador do CGS 21680 na NMT estaria aumentado. Foram realizados registos intracelulares de

potenciais de placa motora (EPPs), potenciais miniatura de placa motora (MEPPs) e potenciais miniatura gigantes de placa motora (GMEPPs) em preparações de nervo frénico-hemidiafragma paralisadas com elevada [Mg^{2+}]. Estímulos de baixa frequência (0.5 Hz) permitiram a avaliação da atividade evocada (EPPs), ao passo que as atividades espontâneas (MEPPs e GMEPPs) foram medidas sem estimulação elétrica. O conteúdo quântico (QC) foi considerado como sendo a razão entre a média da amplitude dos EPPs e média da amplitude dos MEPPs registados no mesmo período de tempo.

Inicialmente validámos o aumento da [Mg^{2+}] como um método útil para o estudo da NMT nos murganhos SOD1G93A. A alteração do equilíbrio entre a razão Ca^{2+}/ Mg^{2+} preservou as características da NMT anteriormente descritas neste modelo.

Na fase pré-sintomática, os animais SOD1G93A apresentaram um aumento na amplitude do EPP e do QC nas concentrações testadas de CGS 21680 quando comparado com murganhos WT ($p<0.05$ *Unpaired t-test*), exceto nas variações do EPP a 3nM ($p>0.05$ *Unpaired t-test*). A amplitude dos MEPPs e GMEPPs não foram alteradas pelo CGS 21680 ($p>0.05$ *Paired t-test*). O aumento na frequência dos MEPPs resultante da ativação dos A2AR não foi significativamente diferente entre os dois grupos na presença de 3 e 10 nM do agonista dos A2AR ($p>0.05$ *Unpaired t-test*) mas foi estatisticamente superior em murganhos SOD1G93A quando perfundido a 5nM ($p<0.05$ *Unpaired t-test*). As NMJs dos animais SOD1G93A pré-sintomáticos apresentaram aumento na frequência dos GMEPPs na presença de CGS 21680 (5 nM) quando comparadas com as dos animais WT ($p<0.05$ *Unpaired t-test*).

Na fase sintomática, o CGS 21680 não alterou a resposta evocada (amplitude dos EPP e QC) nem a atividade espontânea (frequência e amplitude dos MEPPs e GMEPPs) dos animais SOD1G93A ($p>0.05$ *Paired t-test)*. Após estimulação de 0.5 Hz a amplitude dos EPPs, QC e frequência dos MEPPs aumentaram em murganhos WT na presença de 3, 5, 10 e 25 nM de CGS 21680 ($p<0.05$ *Paired t-test)*. Estes parâmetros, juntamente com frequência dos GMEPPs foram significativamente mais elevados do que em murganhos sintomáticos ($p<0,05$ *Unpaired t-test*). A amplitude dos GMEPPs e MEPPs não foram alteradas pela aplicação de CGS 21680 em murganhos WT ($p>0.05$ *Paired t-test)*.

O antagonista dos A2AR SCH 58261 (50nM) não alterou a actividade espontânea e evocada ($p>0.05$ *Paired t-test*) mas bloqueou eficazmente o efeito facilitatório do CGS 21680 (a 5nM em animais de 4-6 semanas e a 10nM em murganhos WT com 12-14 semanas) ($p<0.05$ *Unpaired t-test*).

Os resultados deste estudo apontam para a existência de uma disfunção da modulação adenosinérgica na libertação de ACh antes do aparecimento dos sintomas. Esta disfunção envolve uma sobrerregulação funcional dos A2AR nas NMJs de diafragma de murganhos SOD1G93A pré-sintomáticos.

Quando os sintomas começam a aparecer, a função dos A2AR parece desaparecer em murganhos sintomáticos, mas permanece presente em animais WT de 12-14 semanas de idade. Além disso, o CGS 21680 promoveu uma facilitação A2AR superior em murganhos WT de 12-14 semanas do que de 4-6 semanas. Isto pode ser atribuído a uma característica normal de

maturação da sinapse, contrastando com as observações em animais SOD1G93A.

A passagem de uma sobrerregulação funcional dos A2AR antes da sintomatologia surgir para uma aparente perda da funcionalidade dos A2AR durante a fase sintomática em animais SOD1G93A, destaca o papel deste subtipo de recetores P1 no âmbito da ALS. Tendo isto em consideração, fármacos que atuem nos A2AR poderão eventualmente desempenhar um papel importante no atraso desta doença.

Abbreviations list

A1R - A_1 adenosine receptor

A2AR - A_{2A} adenosine receptor

ACh - acetylcholine

AChE - acetylcholinesterase

ALS - Amyotrophic Lateral Sclerosis

ANOVA - analysis of variance

AP - action potential

ATP - adenosine-5'-triphosphate

cAMP - cyclic adenosine-5'-monophosphate

CGS 21680 - 2-*p*-(2-carboxyethyl) phenethylamino]-5’-N-ethylcarboxamido adenosinehydrochloride

DAG - diacyl glycerol

EMG - electromyography

ER - endoplasmic reticulum

FALS - familial form of Amyotrophic Lateral Sclerosis

FTD - frontotemporal degeneration

FUS - DNA/RNA binding protein fused in sarcoma

GMEPP - giant miniature endplate potential

IgG - immunoglobulin G

IP3 - inositol 1,4,5-trisphosphate

MEPP - miniature endplate potential

MN - motor neuron

MRI - magnetic resonance imaging

nAChR - nicotinic acetylcholine receptor

NMJ - neuromuscular junction

NMT - neuromuscular transmission

PCR - polimerase chain reaction

PKA - protein kinase A

PKC - protein kinase C

PLC - phospholipase C

QC - *quantal content*

SALS - sporadic form of Amyotrophic Lateral Sclerosis

SCH 58261 - 5-Amino-7-(2-phenylethyl)-2-(2-furyl)-pyrazolo(4,3-*e*)-1,2,4-triazolo(1,5-*c*) pyrimidine

SOD1 - superoxide dismutase 1

SOD1G93A - glycine^{93}→alanine point-mutation in human SOD1 protein

TDP-43 - TAR-DNA binding protein 43

VGCC - voltage-gated calcium channel

Wo - weeks old

1. Introduction

1.1. Amyotrophic Lateral Sclerosis

1.1.1. Definition of the disease

Amyotrophic Lateral Sclerosis (ALS) was first described by Charles Bell in 1824. In 1869 the French doctor Jean Marie Charcot established the first pathophysiologic medical definition of the disease. He linked abnormal limb movement to the corticospinal tract pathology and motor neuron (MN) number loss to lower motor degeneration. He then named the disease as ALS incorporating the aspects of gray matter lesion (amyotrophic) and white matter damage (lateral sclerosis) in the spinal cord [1]. Charcot was well aware of the disease fast progression and inability to interfere with its development, a feature that still prevails to this day being ALS one of the major and lethal neurodegenerative diseases.

Despite variable etiology, ALS is considered as a single entity due to a specific recognizable clinical pattern. It is defined as a progressive neurodegenerative disease affecting neuronal cells, in particular MNs. Both upper and lower MNs degenerate leading to progressive denervation of muscle fibers. This results in impairment of neuromuscular transmission (NMT) with subsequent muscle weakness and volume loss. Patients present motor abnormalities with the majority displaying limb weakness as the first sign. ALS evolution will ultimately result in paralysis and patients usually die due to bulbar failure (see [2-3]).

The onset of ALS defines the clinical phenotype, differences in disease severity and life expectancy. Bulbar or spinal dysfunction are considered the

main triggers for ALS associated with a median survival between 3 to 4 years. Bulbar onset represents 25-30% of the cases and is denounced by dysphagia or dysarthria with the last being a strong predictive of impaired locomotion [4]. It is considered the onset with the worst prognosis and usually leads to an earlier respiratory involvement [5]. Limb symptoms (70-75% of all cases) point to a spinal onset that is usually associated with a better prognostic. In 5% of cases patients exhibit a respiratory involvement (see [2-3, 6]).

Prognostic heterogeneity is present in both bulbar and spinal forms of ALS [4]. Sometimes patients can last up to 10 years and exhibit a less severe phenotype. Along with the lack of a specific biomarker, the clinical heterogeneity in ALS remains a challenge and the often used bulbar or spinal distinction may not be adequate. Therefore early diagnosis remains an important feature for prognosis. Due to the overlap with related phenotypes, only well trained clinicians may accurately identify ALS as the cause of MN dysfunction symptoms (see [3, 6]).

1.1.2. Clinical diagnosis

Diagnosis is established by excluding other possible causes of MN disease such as primary lateral sclerosis, progressive muscle atrophy or progressive bulbar palsy. Definite ALS involves both upper and lower MN degeneration and progression of this condition. The diagnostic criteria (El Escorial and Airlie House criteria and the more sensitive Awaji Criteria) are important guidelines and combine several clinical observations in ALS patients towards a correct diagnosis (see [3, 7]).

Tests to rule out the other conditions and confirm ALS include electromyography (EMG), nerve conduction velocity and magnetic resonance imaging (MRI). Blood and urine samples can be used to eliminate the possibility of other diseases (see[3, 7]).

Fasciculations are synonymous of widespread disturbance in membrane excitability and MN degeneration. They are hallmark abnormalities in ALS commonly identified by EMG [8-9]. Motor unit number estimation is also an assessable parameter by EMG that increases certainty in diagnosis ([10] but see [11]). Transmagnetic stimulation may help to unveil upper MN dysfunction. MRI is a neuroimagiological non-invasive technique useful to exclude ALS-like syndromes [3, 7]. Only a combination of these techniques along with monitoring the progress of the disease can account for certainty in clinical diagnosis. With the lack of a specific biomarker the diagnosis is almost exclusively remitted to a symptomatic stage ([12] see [3, 7]).

1.1.3. Epidemiology

New cases are reported every year between 1.5 and 2.5 per 100 000 individuals. 5 to 10% of these cases represent an inherited form of the disease designated familial ALS (FALS) while the other percentage encompasses a sporadic onset (SALS). In SALS, affected individuals start displaying symptoms from 55 to 65 years, while FALS onset starts a decade earlier (see [13]). Some of SALS cases derive from misdiagnosis, poorly ascertained family history and denial thus not reflecting the statistical reality [14]. Mutations arise in several key proteins resulting in disruption of cellular homeostasis capable of triggering

the ALS-phenotype. There are 104 genes with mutations related to the occurrence of ALS [15].

In order to study the biological mechanisms inherent to the disease, transgenic animals have been developed. Mutations from the FALS form of the disease are the basics for the development of these genetic models (see [16]).

1.2. Animal Models of ALS

Mutations of the superoxide dismutase 1 (SOD1) were among the first discovered in FALS patients and the first integrated in a mouse model [17] which became the most studied transgenic rodent model of ALS so far. However, since mutations in the SOD1 gene represented only 20% of FALS and with the discovery of novel genes related with ALS, other models were also developed (see figure 1.3.1). The TAR-DNA binding protein 43 (TDP-43) is a nuclear protein important in gene regulation. It is found co-localized with ubiquitinated inclusions in both SALS and FALS forms and often associated with the Frontotemporal Dementia (FTD) / ALS complex [18-19]. The DNA/RNA binding protein fused in sarcoma (FUS) is a regulator of transcription. Mutations in this protein can lead to ALS in a similar proportion as TDP-43 dysfunction. SOD1, TDP-43 and FUS are considered the most widely accepted ALS-causing genes and therefore the most studied and developed rodent models of the disease (see [20] and [16], [21]).

Recently, the C9*orf*72 gene expansion was found causative of ALS and FTD. This breakthrough in the understanding of ALS etiology highlighted a pleiotropy eventually responsible of triggering different phenotypes (see [22]). The number of repetitions of the C9*orf*72 expansion can account for the severity

and complexity of the disease [21] and may represent a significant percentage of SALS cases [23]. A zebrafish model of ALS has recently putted in evidence the MN deficits behind the aberrant C9*orf*92 expansion [24].

Other genes encoding proteins such as valosine-containing protein, profilin-1 and other proteins have also been related with the occurrence of ALS. This led to the development of new animal models in order to understand the biochemical mechanisms behind this disease in a more broader perspective (see [16]).

1.3. The SOD1G93A mouse as a model to understand ALS

The SOD1 is an ubiquitous enzyme responsible for the catalyzation of reactive oxygen species into hydrogen peroxide in order to prevent oxidative damage events (e.g. lipid peroxidation, DNA damage and apoptosis). There are several mutations in the SOD1 gene that can trigger the ALS-phenotype. The shift in the residue 93 from a glycine into an alanine (SOD1G93A), allows a toxic gain-of-function that gives rise to MN degeneration (see [16, 25]). Since Gurney *et al* (1994) first developed the SOD1G93A mouse it became the most studied model of the disease. One of the major advantages of using this model, is that it highlights developmental pathological features of the neuronal dysfunction (see [26]). This point-mutation in the SOD1 enzyme triggers an intrinsic progression in disease symptomatology in mice, that resembles the clinical variability of ALS .The majority of the findings related to unveiling the cellular dysfunctions as well as the therapeutics trialed in rodent models of ALS were tested in the G93A mutation of the SOD1 gene (see [16]).

In ALS two major stages of disease progression can be distinguished: pre-symptomatic and symptomatic phase. The clear understanding of these

stages in both animal models and humans may reveal fruitful insights of the ALS multifactorial etiology (see [27]) (see table 1.3.I).

1.3.1. Pre-symptomatic ALS: insights from the SOD1G93A mouse

In this rodent model of ALS, symptoms start to arise approximately at 10 weeks of age [17, 28]. Hyperexcitability is a phenomenon that starts long before symptomatology emerges. It can be functionally observed in SOD1G93A motor cortex, spinal cord [29-30] and neuromuscular junction [31]. Cortical hyperexcitability is detectable in pre-symptomatic patients [32] and may contribute to anterior horn excitotoxic cell degeneration (see[33]). An increase in persistent voltage gated sodium channel currents in pre-symptomatic ALS can relate to an endophenotype susceptible to the occurrence of fasciculations in humans and leading to MN excitotoxic death [34]. Reduced inhibitory tonus by alterations in Renshaw cells [35], CB1 receptor trafficking [36] and astrocytic mediators [37] also contributes to hyperexcitability. Indeed, this phenomenon is a strong predictor of survival [38] and may precede ALS onset in patients [39].

Morphologically, SOD1G93A mice start to display MN retraction before symptoms arise with large caliber fibers being the most susceptible [40-41]. Bioenergetic alterations related with mitochrondrial dysfunction may contribute to future functional impairments [42]. Shifting in cellular signaling and gene expression also occurs [43-44].

Studying pre-symptomatic ALS may help to uncover disease-induced maladaptations to ward off symptoms, contributing to the understanding of the full spectrum of ALS degeneration.

1.3.2. Symptomatic ALS: insights from the SOD1G93A mouse

The symptomatic phase is characterized by a selective dysfunction and degeneration of MNs. Axonal transport impairment, activation of microglia, production of toxic factors by glial cells, Ca^{2+} dysfunction and glutamate excitotoxicity are hallmarks of this phase (see[25]). In the motor cortex of ALS patients there is evidence of disconnection along brain networks [45] together with progressive hypometabolism [46]. White and grey matter volume decrease occurs at brain areas of ALS patients (see[47]) which is correlated with observations of global atrophy in the brain and cerebellum of SOD1G93A mice [48]. Impaired oligodendrocyte regeneration in the spinal cord and motor cortex is evident in SOD1G93A mice [49]. Metabolic failures become more severe [50] and accountable for increased energy needs in ALS patients [51].

MN retraction leads to an increment of skeletal muscle fiber atrophy [41] which justifies impairments in NMT and muscle strength loss at this stage [31, 40, 52].

In symptomatic ALS, multifactorial cellular dysfunction is enhanced contributing to the progression of neurodegeneration. This parallels with the evolution of symptoms and results in impairment of motor performance.

Despite some valid criticism (see [2]), the resemblance between SOD1G93A mice characteristics and clinical features of ALS progression validate this rodent model as an actual tool to understand this disease (see[16]).

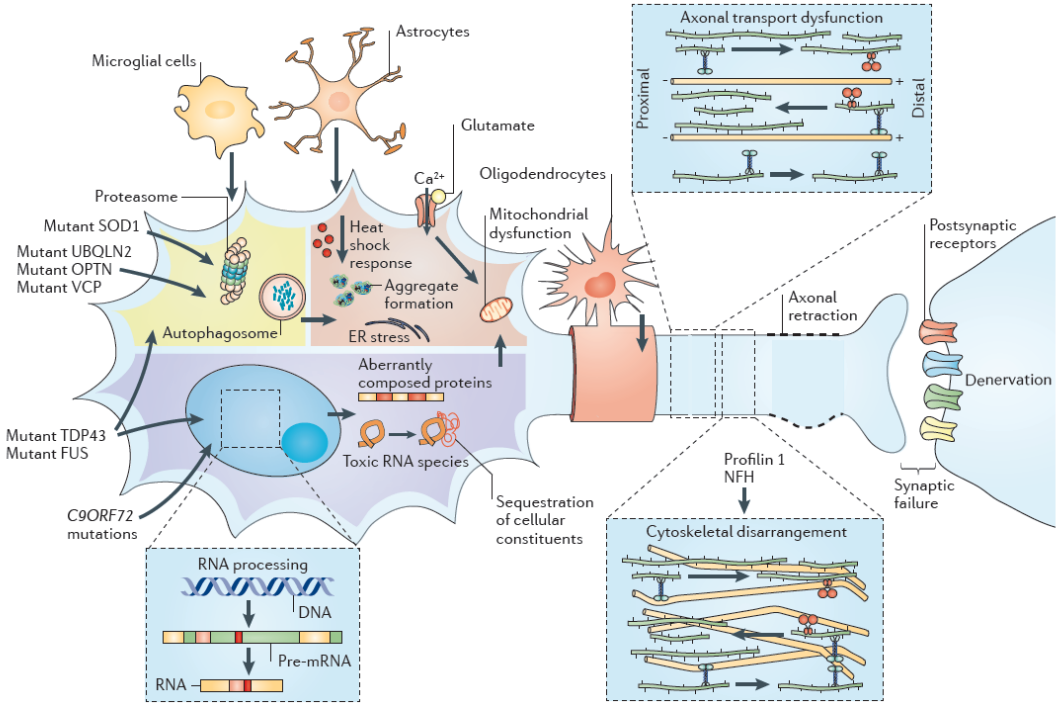

Figure 1.3.1 - Cellular pathological mechanisms of ALS. SOD1 mutations in ALS are responsible for proteossome clogging, axonal transport deficits enhanced by cytoskeletal disarrangement, endoplasmic reticulum (ER) stress and mitochrondrial dysfunction. Mutated SOD1-induced MN retraction will compromise the architecture and functionality of the NMJ. Changes in glial cell function such as astrocytes and microglia can promote increased glutamate excitoxicity and release of inflammatory factors such as Tumor Necrosis Factor α. Other mutations such as C9*orf*72 repeats can directly change the RNA processing quality control, a feature also present in the FUS and TDP-43 mutations [25].

Table 1.3.I - Dysfunctions present in both pre-symptomatic and symptomatic phases of SOD1G93A disease. Information reports observations in the cortex, spinal cord and motor neuron/skeletal muscle of this ALS rodent model.

	Pre-symptomatic	Symptomatic
Cortex	Increased cortical neuron excitability associated with increase persistent Na^+ current [29] Mitochondrial complex activity decrement may induce energy compensation adaptations in the motor cortex [53] Bioenergetic abnormalities at the motor cortex may lead to impairment of corticospinal motor afferents activity [42]	brain and cerebellum atrophy in SOD1G93A rodents [48] deficient oligodendrocyte regeneration in the motor cortex [49]
Spinal Cord	Reduced synaptic input from Renshaw cells leads to lower inhibitory control of motor neuron firing [35] Microglia start to lose synaptic stripping therefore difficulting	Selective accumulation of aberrant SOD1 complexes lead to impaired proteossomal activity [57] Activated microglia releases inflammatory mediators

	neuronal regeneration [54] In the embryonic stages MNs display reduced arborization accountable for functionally hyperexcitability [27-28] Increased microglia expression but not activated microglia [55] Astrocytes release toxic factors that increase excitability in spinal cord cultures [37] Altered functionality of Na^+ channels renders MN susceptible to faster recovery from inactivation [56] Initial astroglyosis at an early symptomatic phase [55]	triggering chemically induced toxicity [55, 58] Mitochondrial dysfunction due to deficient Ca^{2+} buffering, impaired electron transport chain, and induction of apoptosis (see[59]) Dysfunction of astrocytic EAAT2 thus contributing to glutamate excitotoxicity [60] Oligodendrocytes display deficient regeneration [49]
Motor Neuron and Skeletal Muscle	Axonal transport impairment in susceptible MNs by mutant SOD1 interaction with the dynein-dynactin complex [61] Increase of GluR1 and decrease of GluR2 and CB1 receptor trafficking in MNs [36]	Decreased intracellular Ca^{2+} clearance in MNs [63] Impairment of skeletal muscle metabolism may account for failure in energy homeostasis [64]

	Significant end-plate denervation with fast- over slow- fatigable fiber preference [41] Gait abnormalities [52] and atrophy in hindlimb muscles [62] Enhancement of NMT [31]	Presence of a mixed population of NMJs with one group having decrease ACh release [31] Degeneration of neuromuscular synapses and axonal retraction [65] Significant decrease in the number of motor units [28]

1.4. Neuromuscular transmission in ALS: a potential future target?

Since ALS is a progressive neurodegenerative disease affecting MNs, NMT eventually becomes altered. In fact, several morphological and functionally changes in NMJ homeostasis have been identified in both SOD1G93A model [31, 41] and humans [66-68]. Therapies targeting the synapse between motor terminals and end-plates have displayed some success in the rodent model (see [69]), and the study of NMT is a common assessment of treatment effectiveness [70-71].

It is with high priority that one must emphasize NMT modulation as an hypothetical therapeutic strategy in ALS (see [69]). Taking into account the basic principles of cholinergic transmission at the NMJ much can be learn from studying this synapse in ALS models.

1.4.1. Basic concepts on neuromuscular transmission

The NMJ is the synapse between a MN terminal and a specialized region of the muscle fiber designated motor endplate. The action potential (AP) is initiated at the ventral horn of the spinal cord and propagates through the axon. The electric current reaches the terminal of the MN and activates voltage gated calcium channels (VGCC), which are close to release sites, triggering the influx of Ca^{2+} ions into the presynaptic junction. This generates a Ca^{2+} build-up at the terminal activating N-ethylmaleimide-sensitive-factor attachment receptor (SNARE) protein complexes and therefore inducing fusion of acetylcholine (ACh) containing vesicles (see[72]). ACh is co-transmitted with adenosine-5'-triphosphate (ATP) that can act as a neuromodulator at P2 receptors and break

into adenosine which is also a powerful neuroregulator of ACh release at the NMJ [73].

The ACh molecules diffuse through the synaptic cleft and reach the highly invaginated post-synaptic terminal where they interact with the pentameric α1β1ϵγ nicotinic acetylcholine receptors (nAChR). These channels are permeable to Na^+ and in a less degree to Ca^{2+}. Activation of nAChRs generates a flow of current that creates an endplate-potential (EPP). This event, if strong enough, may reach a threshold of depolarization sufficient to trigger a muscular action potential (AP) leading to fiber contraction. ACh action lasts 1ms due to the hydrolytic activity of the acetylcholinesterase enzyme (AChE) that converts ACh into choline and acetate (see [72]).

Single vesicles can be released spontaneously producing a local depolarization - miniature endplate potential (MEPP). If two of more vesicles reach the pos-junctional terminal at the same time, a spontaneous depolarizing event with larger amplitude than a MEPP occurs – Giant miniature end-plate potential (GMEPP). Spontaneous events arise from intracellular Ca^{2+} store mobilization. Since a MEPP corresponds to the amount of ACh molecules per vesicle, the ratio between the EPP/MEPP addresses the *quantal content* (QC), i. e., the number of vesicles released per impulse (see [74-75]).

1.4.2. What do we know about neuromuscular transmission changes in ALS?

Early proof found in muscle preparations of ALS patients, showed atrophic groups of fibers and endplate denervation [66, 76] with evidence of neuronal collateral sprouting [77-78]. High caliber fibers, with higher energetic

demands and large diameter, degenerate first and are re-innervated by low-caliber fiber terminals [41, 79]. This is also evident in the SOD1G93A mouse [41, 62, 80]. Muscle abnormalities result from MN detachment [81] which eventually triggers muscle weakness and atrophy. Muscle overexpression of the neurite outgrowth inhibitor Nogo-A, hypermetabolism leading to energy deficit and signaling deficits account for some of the changes at the NMJ in ALS (see[82-83]).

Immunoglobulins G (IgGs) from ALS patients increased both evoked and spontaneous synaptic transmission at mouse NMJ [67, 84-85] which is consistent with the findings in mice expressing human SOD1 mutations [86]. These IgGs might be uptake by the presynaptic motor terminal [87] and contribute to an increased L-type VGCC blocker sensitivity [88]. These channels contribute to an intraterminal increase of Ca^{2+} levels [89-90]. Deregulation of their function, probably as a versatile compensatory mechanism in pathological conditions [91], could contribute to Ca^{2+}-mediated excitotoxicity, an hallmark in ALS (see [59]).

Recent findings from our group explored the NMT physiology in SOD1G93A mice diaphragm. Boosted ACh release is present in a pre-symptomatic stage with transgenic mice displaying increased QC and increased MEPP and GMEPP frequency. In the later symptomatic stage, two groups of muscle fibers could be separated according to their physiology: one with preserved NMT, and other with decreased QC, MEPP and GMEPP frequency [31]. This postulates the idea that communication between MNs and muscle fibers shifts along disease progression in the SOD1G93A mouse model.

Pharmacological modulation of NMT could hypothetically reveal beneficial in ALS symptomatology.

1.4.3. A_{2A} adenosine receptors: a role for neuromuscular transmission modulation in ALS

In a pharmacological context, the variety of pathological mechanisms in ALS may favor target variety but as a drawback the treatment may lack effectiveness. Riluzole is the only Food and Drug Administration-approved drug to treat ALS. It blocks Tretodotoxin-sensitive voltage gated sodium channels reducing glutamate release. However this mechanism can mitigate excitotoxicity effects prolonging survival only by 2-3 months. One should expect combination therapy as a future successful treatment for ALS symptomatology. This urges the need for the discovery of new viable drugs [92].

Adenosine receptors are G-protein coupled receptors that modulate neurotransmitter release with an high enrollment in pathological conditions. There are 4 types of adenosine receptors - A_1, A_{2A}, A_{2B} and A_3 receptors - that control evoked and spontaneous transmitter release by interaction in both neurons and glial cells. They are activated by adenosine, which can originate from ATP hydrolysis or be released to the extracellular space from the cytoplasm through a nucleoside transporter. The A_1 (A1R) and A_{2A} (A2AR) adenosine receptors are the most prominent P1 neuromodulators in the Central Nervous System with a *via-à-vis* interaction. A1Rs act as depressors of neurochemical release by interacting with $G_{i/o}$ inhibitory proteins leading to a lower probability of transmitter release (see [93]). A2ARs positively modulate adenlytale cyclase via G_s protein activation which results in an increment of

cyclic adenosine monophosphate (cAMP) levels (see [93]). Protein kinase A (PKA) activation is dependent on cAMP. Increased activity of PKA due to A2AR activation promotes recruitment of P/Q-type VGCC and L-type VGCC [91, 94] and negative modulation of K^+ channels. The G_s activation can also activate phospholipase C (PLC), which cleaves phosphatidylinositol 4,5-bisphosphate into diacyl glycerol (DAG) and inositol 1,4,5-trisphosphate (IP3). DAG and Ca^{2+} work together to activate protein kinase C (PKC) a protein that has multiple functions ascribed. IP3 can activate receptors in the endoplasmic reticulum (ER) triggering intracellular pool recruitment of Ca^{2+} (see [93, 95]). Therefore A2AR activation increases the probability of vesicle release leading to higher QC and MEPP frequency [96].

Both receptors are present at the presynaptic junction terminal and modulate ACh release [97]. A1R decreases the cholinergic input while A2AR boosts NMT especially during high-frequency stimulation [91, 98]. In infant rats A2ARs have a preferentially tonic activation over A1R [96] a feature that shifts through ageing [99]. A2AR also facilitate Brain-Derived Neurotrophic Factor actions at the rat NMJ [100].

During the denervation processes of ALS, L-type VGCC recruitment may occur [88] and IgGs from ALS patients can promote Ca^{2+} recruitment trough activation of IP3 and ryanodine receptors (RyR) in MN terminals [101]. Since A2AR activation increases the safety margin at mammalian NMJ (i.e. more *quanta* release per nerve impulse than the necessary to trigger an AP) specially via VGCC recruitment and intracellular store mobilization [102], this receptor could be a valid target for slowing ALS symptomatology. Near-symptomatic administration of CGS 21680 (a selective A2AR agonist) in SOD1G93A mice

increased lifespan and motor performance and postponed disease onset by 12 days [103]. Chronic administration of caffeine (a non-selective antagonist of adenosine receptors) at a similar stage of ALS progression, led to reduced lifespan in the same rodent model highlighting the role of A2ARs in ALS [104].

With the development of adenosine-related drugs in the clinical field (see [105]) and since A2ARs display a specific therapeutic window for neuroprotection in neurodegenerative diseases such as Parkinson and Huntington diseases (see [106]), one should consider adenosinergic modulation as a viable target in experimental models of ALS with potential valid translation into humans.

2. Objectives

Our goal was to functionally assess how the NMT is changed by A2AR activation in high [Mg^{2+}] paralyzed SOD1G93A mouse phrenic nerve-hemidiaphragm preparations. After validating high [Mg^{2+}] as a tool to study NMT modulation in this ALS model, we pharmacologicaly evaluated A2AR functionality through an electrophysiological approach. In order to understand the ALS spectrum of symptom evolution, we conducted the study in both pre-symptomatic and symptomatic stages of the SOD1G93A mouse model in parallel with age-matched control mice.

3. Methods

3.1. Animal model

The SOD1G93A mouse model developed by Guerney *et al.* [17] was used in this study. This is the best-characterized mouse model of ALS and thus the most widely used in research. Mice of this model carry a high copy number (25±1.5) of the human SOD1 gene (transgene) with an autossomical point mutation(glycine^{93}→alanine) which confers an enzymatic toxic gain-of-function responsible for the biological hallmarks of ALS (see [107]).

Transgenic B6SJL-TgN (SOD1-G93A)1Gur/J males (Jackson Laboratory, No. 002726) and wild-type B6SJLF1/J females were purchased from The Jackson Laboratory (Bar Harbor, ME, USA) and were breed at IMM rodent facilities where a colony was established. Mice were maintained on a background B6SJL by breeding SOD1G93A transgenic males with non-transgenic females in a rotational scheme. Males were crossed with non-transgenic females because transgenic females are infertile. F1offspring was used in all experiments. 4-6 and 12-14 weeks old (wo) wild type (WT) animals served as controls. SOD1G93A mice were used to study pre-symptomatic (4-6 wo) and symptomatic (12-14 wo) phases of the disease. Progeny was no longer used in breeding to avoid mSOD1 gene copy number loss and therefore deviation from ALS phenotype [17].

Littermates were identified by dermal ear punching and divided into cages by gender. This method does not require anesthesia and guarantees animal welfare. The ear tissue was used to genotype the animals. Animals were housed 4-5 mice/cage, under a 12h light/12h dark cycle, and received food and

water *ad libitum*. Animals were handled according to European Community guidelines and Portuguese Law on Animal Care.

3.1.1. Genotyping

A polymerase chain reaction (PCR) was conducted on a routine basis to differentiate non-transgenic from SOD1(G93A) transgenic mice in the progeny. The process of genotyping involved several steps namely, DNA extraction, PCR and electrophoresis of PCR products. Wild-type mice present a unique band of 324pb corresponding to the internal positive control. Transgenic mice exhibit an additional band of 236pb corresponding to the SOD1 transgene. Regularly, for quality control purposes, the copy number of F1 transgenic mice was checked through Real time-PCR.

3.2. Electrophysiological Intracellular Recordings

3.2.1. Phrenic-nerve hemidiaphragm preparation

Animals were anaesthetised using halothane and rapidly decapitated. Both right and left phrenic-nerve hemidiaphragms were isolated. One preparation was placed and stretched in a 3mL Perspex chamber (figure 3.2.1) continuously perfused via a roller pump (3mL.min^{-1}) with a physiologic saline solution modified from Krebs and Henseleit (1932) [108](NaCl 117mM; KCl 5mM; $NaHCO_3$ 25mM; NaH_2PO_4 1.2mM; glucose 11mM; $CaCl_2$ 2.5mM; $MgCl_2$ 1.2mM; pH 7,4) continuously gassed with 95% O_2 and 5% CO_2 kept at room temperature (22-25ºC). Muscle stretch does not affect transmitter release at

diaphragm endplates [109]. The other phrenic-nerve hemidiaphragm preparation was kept in a beaker with the saline solution continuously carbogenized until it was mounted in the chamber for experiment.

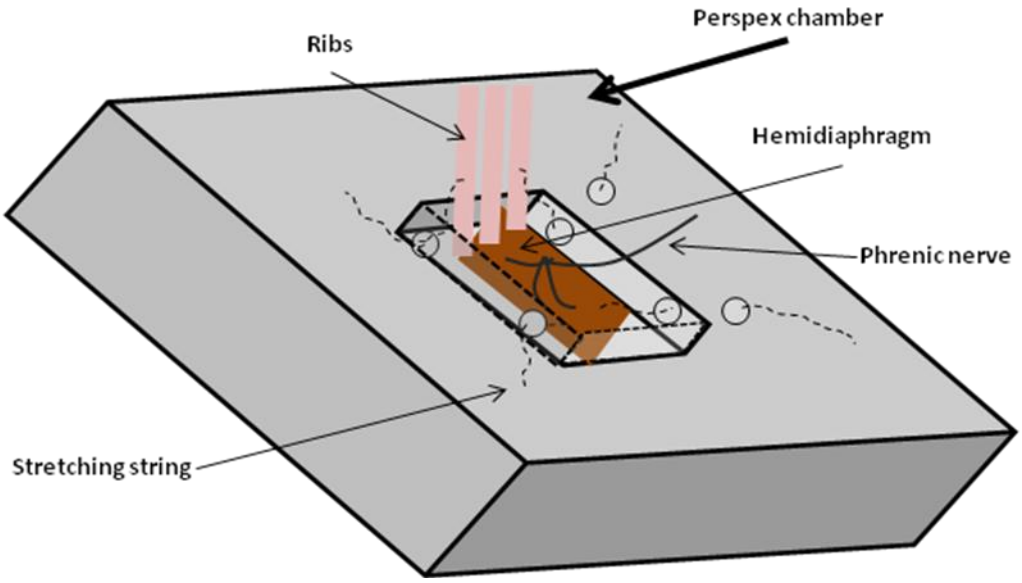

Figure 3.2.1 – schematics of the phrenic-nerve hemidiaphragm preparation in the Perspex chamber. Ribs are isolated together with the muscle and neuronal tissue to help support the preparation in the apparatus. Strings tied to the ribs and to the connective tissue at the end of the hemidiaphragm are used to stretch the preparation in order to avoid mechanical instability and increase muscle surface area.

3.2.2. Electrophysiological setup and intracellular recordings

The phrenic-nerve was stimulated supramaximally by a suction electrode (Cu/Cu^{2+}) connected to a S48 square pulse stimulator (Grass Tecnologies, West Warwick, RI, USA). In order to mimic physiologic conditions of evoked activity, stimuli were applied in a low frequency of 0.5 Hz with a current duration

of 20 µs. Stimulations higher than 1 Hz may induce changes in functional plasticity [110-111]. The reference electrode was an Ag-AgCl pellet placed in the bath. The recording electrode was a glass microelectrode filled with KCl (3 M) with resistance between 15-40 MΩ inserted in the motor endplate site. A Digidata 1440A digitizer (Molecular Devices, Sunnyvale, CA, USA) designed to work with the Axoclamp 2B amplifier (Molecular Devices, Sunnyvale, CA, USA) performed data acquisition (figure 3.2.2). This allowed continuous monitoring and digital storage of EPPs, MEPPs, GMEPPs and resting membrane parameters with adequate software (pCLAMP 10.3, Molecular Devices, Sunnyvale, CA, USA).

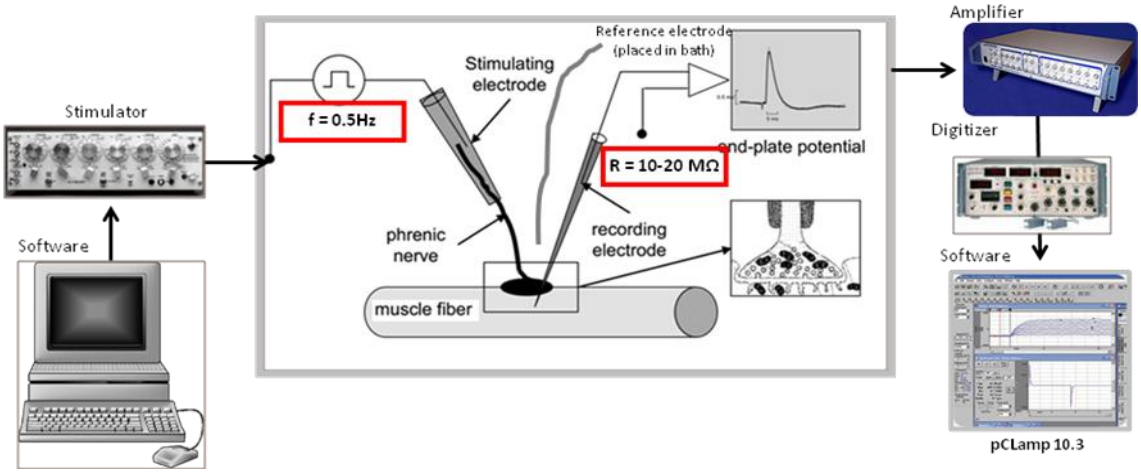

Figure 3.2.2 – Representation of the electrophysiology setup. An interface converts digital signal sent from the computer into analog allowing the stimulator to send command signals. It delivers a direct current through a stimulus isolator resulting in supramaximal square pulses of 20 µs at 0.5 Hz through a stimulating suction electrode. The reference electrode placed in bath allows the measurement of electric activity and resting membrane potential by the recording electrode placed close to the NMJ (<100 µM) [112]. These signals

are sent to the amplifier and then converted into a digital format by the digitizer allowing acquisition by the adequate software.

3.2.3. Increase of Mg^{2+} concentration to block muscle contraction

Muscle twitch can be blocked using 3 pharmacological strategies: (1) submaximal concentrations of tubocurarine which acts as a nAChR blocker allowing visualization of the EPP but not spontaneous activity[113]; (2) increasing the concentration of Mg^{2+} leading to a lower probability of vesicle release[114]; (3) application of μ-conotoxin GIIIB which inhibits muscle type sodium channels preventing the occurrence of an action potential and preserving the QC [115].In this work, Mg^{2+} was added to the physiologic solution to block contraction since this divalent ion can compete with Ca^{2+} in order to lower intraterminal Ca^{2+} influx and therefore keep the EPP below the threshold [114]. Since evoked release is highly dependent on Ca^{2+} micro- and nanodomains build-up at the presynaptic terminal[116], a fine-tuned [Mg^{2+}] ensures the release of enough vesicles to visualize an EPP without the risk of triggering an AP. One must emphasize that it is expected that the increase in [Mg^{2+}] does not significantly change the frequency nor the amplitude of spontaneous events [117], since they are mainly dependent on intracellular Ca^{2+} stores mobilization [118].

In animals 4-6 wo [Mg^{2+}] ranged between 18.5-19.5 mM. Higher concentrations resulted in EPPs lower than 1mV which could be more prone to signal contamination and a potential bias in data off-line analysis. Contraction in

older animals (12-14 wo) was blocked by 20.0-22.0 mM of magnesium (figure 3.2.3).

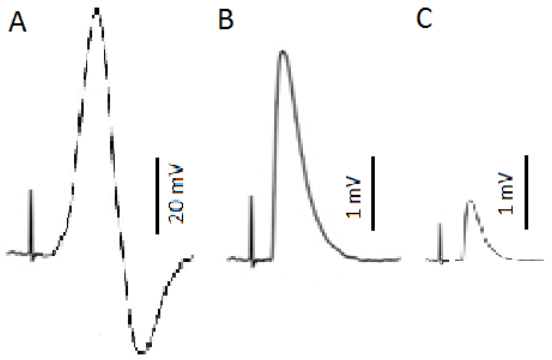

Figure 3.2.3 – representation of the possible evoked events displayed at stimulated NMJs while determining a fine range of [Mg^{2+}] to block contraction. (A) low concentrations of Mg^{2+} (<18.5 mM in 4-6 wo and <20.0 mM in 12-14 wo animals) can lead to EPPs in some fibers reaching the threshold to trigger an AP not allowing a stable resting membrane potential and the fiber twitch can crush the tip of the glass microelectrode; (B) the specific range of [Mg^{2+}] for each phase of the study, in the large majority of the fibers, leads to EPPs greater than 1 mV and lower than 5 mV and a stable membrane potential; (C) concentrations too high of the Ca^{2+} competitor (>19.5 mM in 4-6 wo and >22.0 mM in 12-14 wo animals) will result in EPPs lower than 1 mV which difficults drug assay.

3.3. Electrophysiological parameters

Cell viability and recording precision was determined by 3 important factors: (1) stable resting membrane potential throughout all experiment without

less than 5% variation of its initial value. Fibers with a resting potential between -65 to -85 mV were chosen; (2) basal noise lower than the amplitude of any spontaneous event at the recording fiber; (3) mean EPP amplitude constant before adding any drug. Clogging of the recording electrode was denounced by increase in basal noise, change in electrode resistance, and sudden shift in resting membrane potential. A brief pulse of current could be used to unclog the electrode and if all the parameters remained stable before the obstruction of the tip of the glass micropipette the experiment could continue.

3.3.1. Evoked activity

EPPs were evaluated as the average of the amplitude of 60 consecutive EPPs with amplitude ranging between 1mV to 5 mV. The mean of the average of the EPP amplitude in the last 10 minutes before adding any drug were compared with the last 10 minutes of drug perfusion to evaluate the percentage of drug effect. Drug perfusion lasted 34 to 40 minutes.

QC can be used to indicate the number of vesicles released per evoked impulse. In Mg^{2+} blocked preparations QC is generally less than 5 and the accuracy of its calculation carries no small fluctuations [117]. It is calculated by the ratio between the mean EPP amplitude and the mean MEPP amplitude acquired during the same period with the same resting membrane potential.

$$\text{mean QC} = \frac{\text{mean EPP amplitude}}{\text{mean MEPP amplitude}}$$

3.3.2. Spontaneous activity

MEPPs were recorded in gap-free intervals of 100 seconds before adding the drug and at the end of drug perfusion. MEPP threshold of detection

was set between 0.2 mV and 1.5 mV (see section 4.1.1.2 and 4.1.2.2). In these periods amplitude was defined as the mean of all spontaneous events and the frequency as the number of events.

Since GMEPP amplitude is at least the double of a MEPP amplitude [119], the minimum GMEPP threshold amplitude was set in 1.5 mV (see section 4.1.1.2 and 4.1.2.2). This indirect measure of spontaneous activity synchronism was analyzed as the frequency of giant events in the 100 seconds gap-free acquisition mode and the mean amplitude as the average of GMEPP magnitude in the same interval.

In the analysis of the NMT physiology of in high [Mg^{2+}] paralyzed preparations (section 4.1), we also studied the rise and decay times and area of both GMEPPs and MEPPs. MEPP rise and decay times are also punctually explored in the A2AR modulation study (see section 4.2.1.2).

In the off-line analysis a Gaussian lowpass filter (-3dB cutoff = 600 Hz) was applied and electric interference was removed using the Clampfit software (Molecular Devices, Sunnyvale, CA, USA) (figure 3.3.1). After exporting the data file to an *integer* format, frequency, amplitude, rise and decay times and area were analyzed with Mini-Analysis software (Synaptosoft Inc., Decatur, GA, USA).

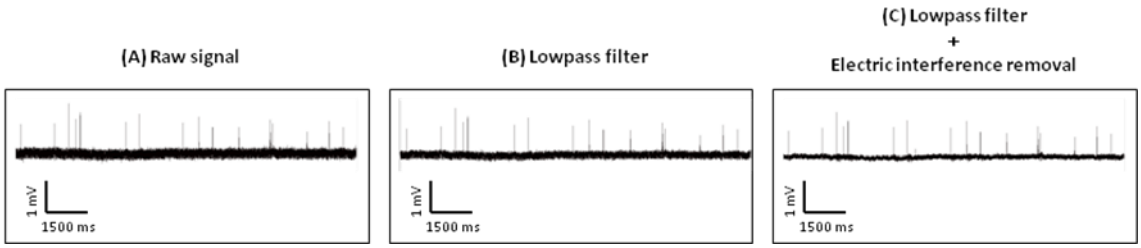

Figure 3.3.1 – several filters applied in the off-line analysis of spontaneous events. **(A)** signal without any filter; **(B)** signal with a lowpass filter applied and **(C)** plus the removal of electric interference. One can notice that both signal amplitude and frequency remain unchanged during this process of digital analysis.

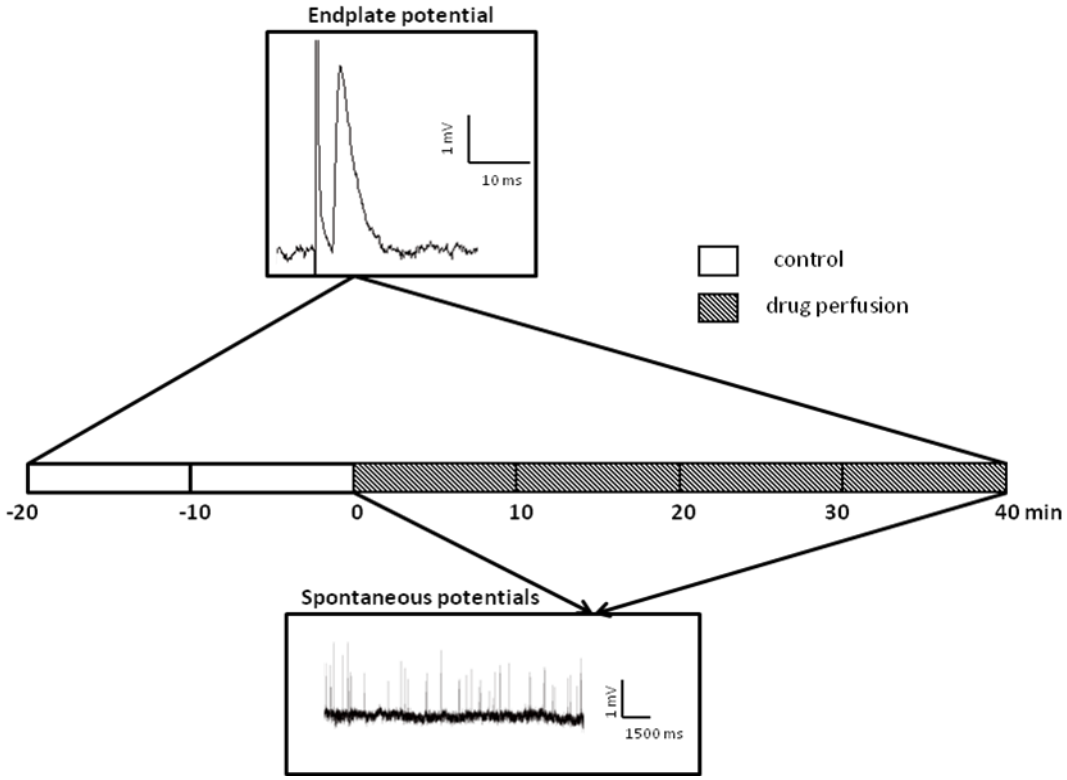

Figure 3.3.2 – schematic representation of the timeline of events analyzed during an experiment. After having a stable NMJ for at least 20 to 30 minutes, spontaneous activity is recorded during 100 sec without stimulation. Then the pump inlet tube is transferred from one flask to another to change solutions and

start drug perfusion (30 to 40 minutes). This change, if done carefully, does not trigger any disturbance to the preparation allowing many changes if needed. Then, evoked activity (EPPs) and spontaneous activity (MEPPs and GMEPPs) are recorded.

3.4. Drugs

To evaluate A2AR modulation, agonist and antagonist were used (see table 3.4.I). The A2AR selective agonist (CGS 21680) was perfused alone or in the presence of the A2AR antagonist (SCH 58261). The A2AR blocker was perfused at least 30 minutes before addition of CGS 21680. All stock solutions were made in dimethyl sulfoxide, which is used as a common procedure to dissolve compounds for biological assays. To avoid compound precipitation aliquots were kept frozen at -20ºC until used [120]. Dimethyl sulfoxide was devoid of effect in the performed experiments like previously reported [99-100].

Table 3.4.I – Description of the A2AR-related drugs used in this study

Designation	Abbreviation	Function	Supplier	Binding affinity (nM)
2-*p*-(2-carboxyethyl) phenethylamino]-5'-N-ethylcarboxamido adenosinehydrochloride	CGS 21680	A_{2A} adenosine receptor agonist	Tocris (Bristol, UK)	Ki_{A1}=2600 Ki_{A2A}=15 [121]

5-Amino-7-(2-phenylethyl)-2-(2-furyl)-pyrazolo(4,3-*e*)-1,2,4-triazolo(1,5-*c*) pyrimidine	SCH 58261	A_{2A}adenosine receptor antagonist	Tocris (Bristol, UK)	Ki_{A1}=800 Ki_{A2A} =1.2[122]

3.5. Statistical analysis

Data is reported as mean ± standard error mean. In the evaluation of the physiology of NMT in the presence of high [Mg^{2+}] (section 4.1) the number of mice and number of fibers is discriminated. In the A2AR experiments (section 4.2) each number corresponds to the amount of animals used (1 fiber per mouse).

In the study of section 4.1, three statistic tests were used: Student's *t*-test for independent samples with normal distributions with homogeneous variances (Unpaired *t*-test); Mann-Whitney *U*-test when a group displayed a non-normal distribution; Student's *t*-test with Welch's correction whenever variances were heterogeneous. Saphiro-Wilk test was used to test normality and homogeneity of variances was verified with F-test. Significance was settled at $p<0.05$ in all cases.

Non-linear regression was used to underline the differences in MEPP amplitude distribution. A gaussian curve best fitted the model.

In section 4.2 to verify differences in drug effect between the two groups (WT and SOD1G93A) at the same concentration of the A2AR agonist, the Student's *t*-test for independent samples (Unpaired *t*-test) was applied. When comparing more than 2 means one-way analysis of variance (ANOVA) was performed. If $p<0.05$, Tukey's pos-test was applied to compare drug-induced changes between different groups. Student's *t*-test for paired samples (Paired *t*-test) was applied to compared obtained data with the measured parameter before adding the drug (e.g. EPP mean amplitude before CGS 21680 perfusion). Differences were considered significant whenever $p<0.05$.

4. Results

4.1. Physiology of the neuromuscular transmission in SOD1G93A mice in the presence of high [Mg^{2+}]

We first accessed the physiology of the NMT in the presence of high [Mg^{2+}]. Our purpose was to verify if changes in the Ca^{2+}/Mg^{2+} ratio interfered with the evoked or spontaneous release of ACh in 4-6 wo and 12-14 wo animals previously characterized by our group with μ-conotoxin GIIIB paralyzed preparations [31].

4.1.1. Pre-symptomatic phase

4.1.1.1. Evoked activity

Evoked response (QC and EPP) results are illustrated in table 4.1.I. EPP amplitude in WT (2.19±0.18mV) was not statistically different to that displayed by pre-symptomatic transgenic mice (2.23±0.16mV) ($p>0.05$ Unpaired *t*-test). The QC was also statistically identical between both groups of animals (2.96±0.20 in WT and 2.81±0.18 in SOD1G93A mice) ($p>0.05$ Unpaired *t*-test). The resting membrane potential was close to -75mV (see section 4.1.1.2).

Table 4.1.I – Evoked activity of 4-6 wo WT and pre-symptomatic SOD1G93A mice in the presence of high [Mg^{2+}].

	4-6 wo mice	
n (mice, fibers)	WT (18, 29)	SOD1G93A (22, 34)
EPP (mV)	2.19±0.18	2.23±0.16
QC	2.96±0.20	2.81±0.18

4.1.1.2. Spontaneous activity

MEPPs and GMEPPs can be differentiated based on their amplitude [119]. Figure 4.1.1A displays the frequency histogram of the amplitude of all spontaneous events in both WT and SOD1G93A mice. These events fit in a Gaussian curve (figure 4.1.1B) like previously described [31] (R^2=0.92 for WT and R^2=0.92 for SOD1G93A). According to this non-linear regression analysis, spontaneous events between 0.6 and 0.8 mV were the most frequent.

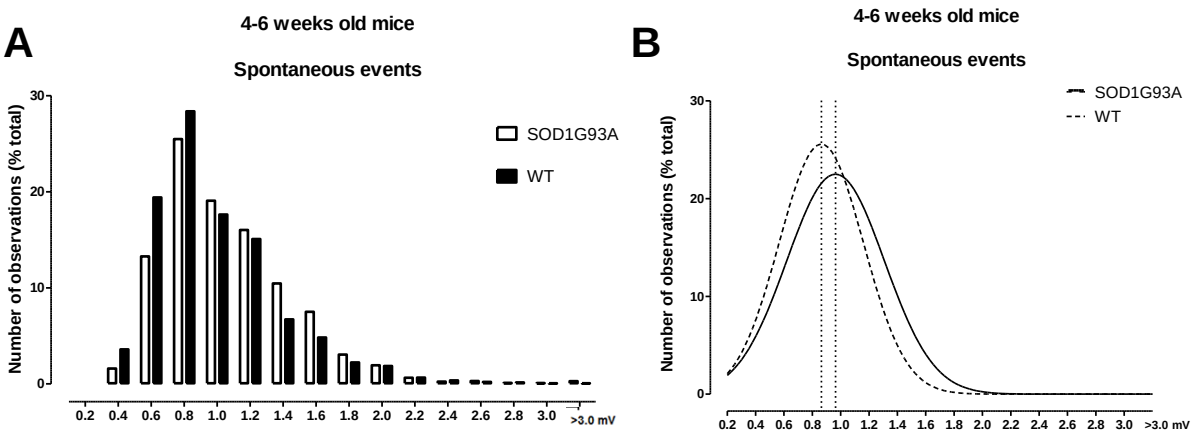

Figure 4.1.1 – **(A)** frequency histogram of distributed spontaneous events from WT and SOD1G93A mice. Events between 0.6 and 0.8 mV are the most frequent; **(B)** Gaussian distribution of the amplitude from spontaneous events in both animal groups (n=18, 29 fibers, WT; n=22, 34 fibers, SOD1G93A)

Table 4.1.II displays the parameter analysis from spontaneous activity in 4-6 wo animals. Resting membrane potentials were relatively close to -75mV in both animal groups (-75.96±0.97mV, WT; -77.36±0.69mV, SOD1G93A). MEPP frequency was not different in both groups (0.97±0.06s^{-1}, WT; 0.96±0.06s^{-1}, SOD1G93A; p>0.05 Mann-Whitney *U*-test) but MEPP amplitude was significantly increased in SOD1G93A mice (0.828±0.036mV, WT; 0.940±0.03mV, SOD1G93A; p<0.05 following Unpaired *t*-test). Rise and decay times in WT mice (2.79±0.10ms) when compared with SOD1G93A mice

(2.70±0.07ms) together with MEPP decay time (11.50±0.3 ms, SOD1G93A; 12.35±0.40ms, WT) were not statistically different (p>0.05 Mann-Whitney *U*-test). MEPP area evidenced no significant variation when comparing both groups (4.25±0.21, WT; 4.07±0.16, SOD1G93; p>0.05 Mann-Whitney *U*-test).

Regarding GMEPPs, table 4.1.II shows that these events were present in 20 out of 29 fibers studied in WT mice (≈69%). In SOD1G93A mice the number of muscle fibers with GMEPPs was slightly higher, with 26 of the 34 fibers analyzed (≈76%) having spontaneous post-synaptic potentials where 2 or more ACh vesicles reached the post-synaptic terminal simultaneously. GMEPP amplitude (1.904±0.068mV, WT; 1.885±0.070mV, SOD1G93A) and frequency (0.09±0.03s^{-1}, WT; 0.11±0.03s^{-1}, SOD1G93A) did not differ significantly between both groups (p>0.05 Unpaired *t*-test). The GMEPP rise time was significantly slower in WT mice (4.31±0.40ms) than in SOD1G93A mice (3.19±0.20ms) (p<0.05 Student's *t*-test with Welch's correction). GMEPP area in SOD1G93A mice (9.47±0.78), was higher than WT mice (11.90±1.11) (p<0.05 Mann-Whitney *U*-test).

Table 4.1.II – Spontaneous activity of pre-symptomatic SOD1G93A mice and 4-6 wo WT mice in the presence of high [Mg^{2+}].

	4-6 wo mice	
n (mice, fibers)	WT (18, 29)	SOD1G93A (22, 34)
Resting membrane potential (mV)	-75.96±0.97	-77.36±0.69
MEPP frequency (s^{-1})	0.97±0.06	0.96±0.06
MEPP amplitude (mV)	0.828±0.036	0.940±0.03*
MEPP Rise Time (ms)	2.79±0.10	2.70±0.07
MEPP Decay Time (ms)	12.35±0.40	11.50±0.32
MEPP Area	4.25±0.21	4.07±0.16

Nº of fibers with GMEPPs	20	26
GMEPP amplitude (mV)	1.904±0.068	1.885±0.070
GMEPP frequency (s^{-1})	0.09±0.03	0.11±0.03
GMEPP Rise Time (ms)	4.31±0.40	3.19±0.20[#]
GMEPP Decay Time (ms)	17.62±1.34	15.57±1.22
GMEPP Area	11.90±1.11	9.47±0.78[+]

*p<0.05 Unpaired *t*-test

[#]p<0.05 Student's *t*-test with Welch's correction

[+]p<0.05 Mann-Whitney *U*-test

4.1.2. Symptomatic phase

4.1.2.1. Evoked activity

We can observe in table 4.1.III that EPP amplitude did not significantly differ between WT and SOD1G93A groups (2.66±0.25mV, WT; 2.91±0.25mV, SOD1G93A; p>0.05 Unpaired *t*-test). QC was slightly increased in SOD1G93A mice (4.42±0.33) when compared to WT (3.93±0.37) but not significantly (p>0.05 Mann-Whitney *U*-test). Resting membrane potential was close to -75mV (see section 4.1.2.2).

Table 4.1.III - Evoked activity of 12-14 wo WT and symptomatic SOD1G93A mice in the presence of high [Mg^{2+}].

	12-14 wo mice	
n (mice, fibers)	WT (19, 24)	SOD1G93A (16, 22)
EPP (mV)	2.66±0.25	2.91±0.25
QC	3.93±0.37	4.42±0.33

4.1.2.2. Spontaneous activity

Figure 4.1.2A represents the histogram of the distribution of the amplitude of all spontaneous events analyzed in 12-14 wo animals. A shift between WT and SOD1G93A mice spontaneous activity amplitude can be observed in the Gaussian curve (figure 4.1.2B), evidenced by a pronounced skewing to the right in WT mice.

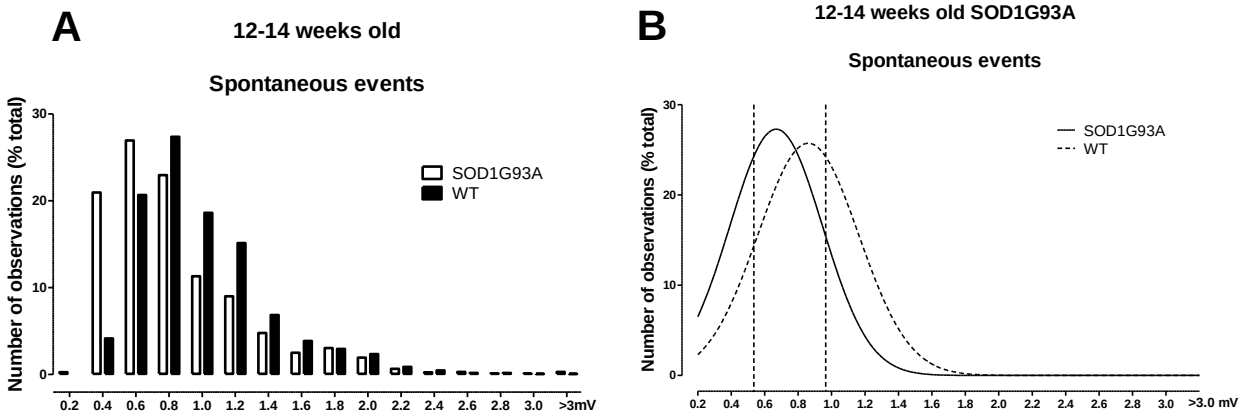

Figure 4.1.2 – **(A)** histogram representation of 12-14 wo WT and symptomatic SOD1G93A mice spontaneous events amplitude; **(B)** Gaussian curve representing the distribution of spontaneous events, showing a skewing to the right in WT events when compared to SOD1G93A distribution; (n=19, 24 fibers, WT; n=16, 22 fibers, SOD1G93A).

Comparing these groups (table 4.1.IV), we can observe that SOD1G93A mice had statistically lower MEPP amplitude than WT mice (0.907±0.044mV, WT; 0.663±0.05mV, SOD1G93A; $p<0.05$ Mann Whitney *U*-test). MEPP frequency is higher in 12-14 wo WT mice (1.52±0.46s^{-1}, WT; 1.07±0.16s^{-1}, SOD1G93A; $p<0.05$ Mann Whitney *U*-test) and MEPP area is decreased in transgenic mice (4.09±0.25, WT; 3.05±0.22, SOD1G93A; $p<0.05$ Unpaired *t*-test). MEPP rise and decay times were not significantly different between

groups (p>0.05 Mann-Whitney *U*-test). 15 out of 24 fibers analyzed from WT animals (≈63%) had GMEPPs while only 6 of the 22 fibers from SOD1G93A mice (≈27%) had giant spontaneous events. SOD1G93A mice presented higher mean GMEPP amplitude (1.753±0.068mV, WT; 1.997±0.168mV, SOD1G93A), mean decay time (15.15±0.96ms, WT; 18.71±3.88ms, SOD1G93A) and mean area (8.28±0.51, WT; 9.16±0.42, SOD1G93A) but without statistical significance (p>0.05 Unpaired *t*-test). GMEPP rise time was significantly different between both groups (2.95±0.32ms, WT; 5.29±0.65ms; SOD1G93A; p<0.05 Unpaired *t*-test).

Table 4.1.IV - Spontaneous activity of symptomatic SOD1G93A mice and 12-14 wo WT mice in the presence of high [Mg^{2+}]

	12-14 wo mice	
n (mice, fibers)	WT (19, 24)	SOD1G93A (16, 22)
Resting membrane potential (mV)	-75.96±0.97	-77.36±0.69
MEPP frequency (s^{-1})	1.52±0.46	1.07±0.16^{+}
MEPP amplitude (mV)	0.907±0.044	0.663±0.05^{+}
MEPP Rise Time (ms)	2.64±0.11	2.74±0.13
MEPP Decay Time (ms)	11.13±0.51	10.47±0.43
MEPP Area	4.09±0.25	3.05±0.22*
Nº of fibers with GMEPPs	15	6
GMEPP amplitude (mV)	1.753±0.068	1.997±0.168
GMEPP frequency (s^{-1})	0.13±0.03	0.07±0.03
GMEPP Rise Time (ms)	2.95±0.32	5.29±0.65*
GMEPP Decay Time (ms)	15.15±0.96	18.71±3.88
GMEPP Area	8.28±0.51	9.16±0.42

*p<0.05 Unpaired *t*-test

+p<0.05 Mann-Whitney *U*-test

4.1.3. Comparison between phases

4.1.3.1. Evoked activity

In WT mice, EPP amplitude did not vary statistically between 4-6 and 12-14 wo animals (2.19±0.18mV, 4-6 wo WT; 2.66±0.25mV, 12-14 wo WT; $p>0.05$ Mann Whitney *U*-test). QC was significantly increased in older animals (2.96±0.20, 4-6 wo WT; 3.93±0.37, 12-14 wo WT; $p<0.05$ Mann Whitney *U*-test) (see table 4.1.VI).

Table 4.1.VI- Comparison of EPP amplitude and QC between 4-6 and 12-14 wo WT mice

	12-14 wo mice	
	4-6 wo WT	12-14 wo WT
n (mice, fiber)	(18, 29)	(19, 24)
EPP (mV)	2.19±0.18	2.66±0.25
QC	2.96±0.20	3.93±0.37^{+}

$^{+}p<0.05$ Mann-Whitney *U*-test

In transgenic mice, both EPP amplitude and QC were significantly reduced in pre-symptomatic SOD1G93A mice in comparison with older ALS mice (2.23±0.16mV and 2.81±0.18mV, respectively in pre-symptomatic SOD1G93A; 2.91±0.25mV and 4.42±0.33mV, symptomatic SOD1G93A; $p<0.05$ Mann-Whitney *U*-test) (see table 4.1.VII).

Table 4.1.VII - Comparison of EPP amplitude and QC between pre-symptomatic and symptomatic SOD1G93A mice

	12-14 wo mice	
	Pre-symptomatic SOD1G93A	Symptomatic SOD1G93A
n (mice, fiber)	(22, 34)	(16, 22)
EPP (mV)	2.23±0.16	2.91±0.25^{+}
QC	2.81±0.18	4.42±0.33^{+}

$^{+}$p<0.05 Mann-Whitney *U*-test

4.1.3.2. Spontaneous activity

Table 4.1.VIII- Comparison of the parameters obtained from spontaneous activity analysis of 4-6 and 12-14 wo WT mice

	4-6 wo WT	12-14 wo WT
n (mice, fiber)	(18, 29)	(19, 24)
MEPP frequency (s^{-1})	0.97±0.06	1.52±0.46^{+}
MEPP amplitude (mV)	0.828±0.036	0.907±0.044
MEPP Rise Time (ms)	2.79±0.10	2.64±0.11
MEPP Decay Time (ms)	12.35±0.40	11.13±0.51
MEPP Area	4.25±0.21	4.09±0.25
Nº of fibers with GMEPPs	20	15
GMEPP amplitude (mV)	1.904±0.068	1.753±0.068
GMEPP frequency (s^{-1})	0.09±0.03	0.13±0.03
GMEPP Rise Time (ms)	4.31±0.40	2.95±0.32*
GMEPP Decay Time (ms)	17.62±1.34	15.15±0.96
GMEPP Area	11.90±1.11	8.28±0.51^{+}

*p<0.05 Unpaired *t*-test

$^{+}$p<0.05 Mann-Whitney *U*-test

Table 4.1.VIII displays the comparison of the spontaneous activity between 4-6 weeks and 12-14 wo WT mice. MEPP frequency was significantly increased in older animals (0.97±0.06s^{-1}, 4-6 wo WT; 1.52±0.46s^{-1}, 12-14 wo WT, p<0.05 Mann-Whitney *U*-test). GMEPP area was statistically increased in

12-14 wo WT mice (11.90±1.11, 4-6 wo WT; 8.28±0.51, 12-14 wo WT; p<0.05 Mann-Whitney U-test) and rise time was significantly faster in older animals (4.31±0.40ms; 4-6 wo WT; 2.95±0.32ms, 12-14 wo WT; p<0.05 Unpaired *t*-test).

Table 4.1.IX- Comparison of MEPP evaluated parameters between pre-symptomatic and symptomatic SOD1G93A mice

	SOD1G93A	
n (mice, fibers)	Pre-symptomatic (22, 34)	Symptomatic (16, 22)
Resting membrane potential (mV)	-77.36±0.69	-77.36±0.69
MEPP frequency (s^{-1})	0.96±0.06	1.07±0.16
MEPP amplitude (mV)	0.940±0.03*	0.663±0.05$^{\#}$
MEPP Rise Time (ms)	2.70±0.07	2.74±0.13
MEPP Decay Time (ms)	11.50±0.32	10.47±0.43
MEPP Area	4.07±0.16	3.05±0.22$^{\#}$
Nº of fibers with GMEPPs	15 (24)	6 (22)
GMEPP amplitude (mV)	1.753±0.068	1.997±0.168
GMEPP frequency (s^{-1})	0.13±0.03	0.07±0.03
GMEPP Rise Time (ms)	2.95±0.32	5.29±0.65*
GMEPP Decay Time (ms)	15.15±0.96	18.71±3.88
GMEPP Area	8.28±0.51	9.16±0.42

*p<0.05 Unpaired *t*-test

$^{\#}$p<0.05 Student's *t*-test with Welch's correction

In ALS mice, symptomatic SOD1G93A animals presented significantly lower MEPP amplitude than pre-symptomatic SOD1G93A mice (0.940±0.03mV, pre-symptomatic SOD1G93A; 0.663±0.05mV, symptomatic SOD1G93A; p<0.05 Student's *t*-test with Welch's correction) and smaller MEPP area (4.07±0.16, pre-symptomatic SOD1G93A; 3.05±0.22, symptomatic SOD1G93A, p<0.05 Student's *t*-test with Whelch's correction) (see table 4.1.IX).

Regarding GMEPPs, overall comparison between pre- and symptomatic SOD1G93A mice suggested a higher prevalence of GMEPPs in the former (≈63% versus 27% in symptomatic SOD1G93A) and slower GMEPP rise time in symptomatic SOD1G93A mice (2.95±0.32ms, pre-symptomatic SOD1G93A; 5.29±0.65ms, symptomatic SOD1G93A; $p<0.05$ Unpaired *t*-test) (see table 4.1.IX).

4.2. Effect of adenosine A_{2A} receptors on the neuromuscular transmission of ALS mice

The A2AR functionality was assessed in both phases of disease progression in pre- and symptomatic SOD1G93A mice and in 4-6 wo and 12-14 wo WT mice. In order to evaluate how A2AR modulate NMT at phrenic-nerve hemidiaphragm preparations, we performed dose-response experiments with the A2AR selective agonist CGS21680 [121] at 3, 5 and 10 nM in WT and SOD1G93A mice. We used CGS 21680 (25nM) in the older groups of rodents (12-14 wo animals) to unveil if A2AR facilitation could be augmented at concentrations higher than 10nM (see section 4.2.2).

4.2.1. Pre-symptomatic phase

4.2.1.1. Evoked activity

Figure 4.2.1A displays the effect of CGS21680 in EPP amplitude at the 3 tested concentrations i.e. 3, 5 and 10 nM. At 3nM the A2AR agonist displayed a higher facilitation in SOD1G93A (16.60±2.73%, n=5) than WT mice (8.97±1.85%, n=7) but no statistical significance was found ($p>0.05$ Unpaired *t*-test). Using 5 nM of CGS21680, NMT was largely enhanced in transgenic

animals when compared to WT (8.54±1.24% n=8, WT, 26.56±3.33%, n=15, SOD1G93A, p<0.05 Unpaired *t*-test). The same feature was present when 10 nM of CGS21680 was applied (5.59±0.99%, n=4, WT, 19.19±4.07%, n=5, SOD1G93A, p<0.05 Unpaired *t*-test). When using 5 nM of CGS 21680, EPP increase in the SOD1G93A group was higher than in the other concentrations (3 and 5nM of CGS 21680). In WT mice CGS 21680 effect was similar at 3 and 5 nM but slightly decreased at 10 nM. However differences in concentration-dependent effect were not significantly different within the same group (p>0.05 one-way ANOVA**).** Taking this into account, we selected CGS 21680 at 5nM whenever a more profound study of the A2AR functionality was needed in 4-6 wo mice (e.g. evaluation of the A2AR antagonist effect). Due to a typical patchiness in CGS 21680 responses on NMT [97] a higher number of experiments was performed at this concentration. In figure 4.2.1B we can see the different effect in EPP amplitude upon A2AR activation by CGS21680 (5nM), in both WT and SOD1G93A groups throughout drug perfusion.

In order to determine if the observed effect was via A2AR activation, we used the A2AR antagonist (SCH 58261) [122] combined with 5nM of the A2AR agonist. In 4-6 wo WT animals, SCH 58261 (50nM) exhibited no significant effect in EPP amplitude (-2.33±1.58%, n=5; p>0.05 Paired *t*-test) and effectively blocked CGS21680 (5nM) effect (2.27±1.10%, n=5) (p<0.05 one-way ANOVA followed by Tukey's pos-hoc) (see figure 4.2.1C). In SOD1G93A animals, the A2AR antagonist effect was null (2.00±1.05%, n=6; p>0.05 Paired *t*-test) and significantly blocked A2AR facilitation by CGS21680 (5nM) (0.39±1.17%, n=5) (p<0.05 one-way ANOVA followed by Tukey's pos-hoc). These results ensured that CGS21680 action was trough A2AR activation.

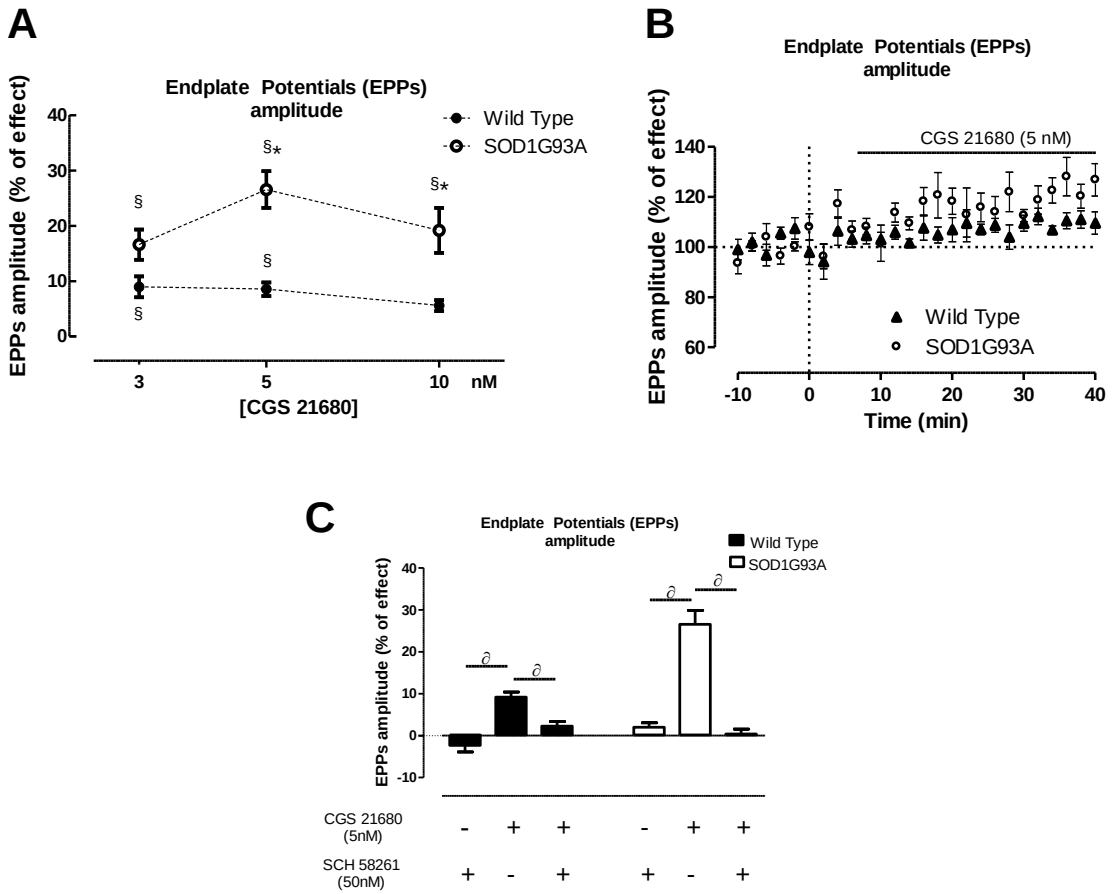

Figure 4.2.1- (A) dose-response change in EPP amplitude in the presence of CGS21680 (3 nM: n=7, WT, n=5, SOD1G93A; 5nM: n=8, WT, n=15, SOD1G93A; 10nM: n=4, WT, n=5, SOD1G93A); **(B)** representative averaged changes in EPP amplitude in the presence of 5nM of CGS 21680 (n=4, WT, n=6 SOD1G93A); **(C)** bar-representation of CGS 21680 (5nM) and SCH 58261 (50nM) interaction in EPP amplitude (SCH 58261 at 50 nM: n=5, WT, n=6, SOD1G93A; CGS 21680 (5nM) in the presence of SCH 58261 (50nM): n=5, WT; n=5, SOD1G93A); § Paired *t*-test (as compared with mean EPP amplitude before drug perfusion); $^{\partial}p<0.05$ one-way ANOVA followed by Tukey's pos-hoc, *p<0.05 Unpaired t-test.

QC increase in SOD1G93A was higher than in WT in all concentrations of CGS 21680 (Figure 4.2.2A). QC was significantly higher in transgenic when

compared to WT animals at 3nM (9.41±3.22%, n=5, WT, 21.20±1.78%, n=4, SOD1G93A), 5 nM (9.46±2.20%, n=8, WT, 27.73±4.15%, n=10, SOD1G93A) and 10 nM of the A2AR agonist. (4.61±1.23%, n=4, WT, 22.29±6.07%, n=4, SOD1G93A) ($p<0.05$ Unpaired *t*-test). At 3, 5 and 10nM of CGS 21680, QC was significantly different from control situation (mean QC before adding the drug), however in WT mice this was only evident when 3 and 5nM of the drug were applied ($p<0.05$ Paired *t*-test).

SCH 58261 at 50 nM significantly blocked the CGS21680 effect on QC increase in WT (-2.01±1.30%, n=4) and SOD1G93A mice (0.88±1.73%, n=6) ($p<0.05$ one-way ANOVA followed by Tukey's pos-hoc) and *per se* was devoid of effect in QC in both phenotypes (-1.83±3.34%, n=4, WT, 3.16±1.13%, n=5, SOD1G93A; $p>0.05$ Paired *t*-test) (see figure 4.2.2B).

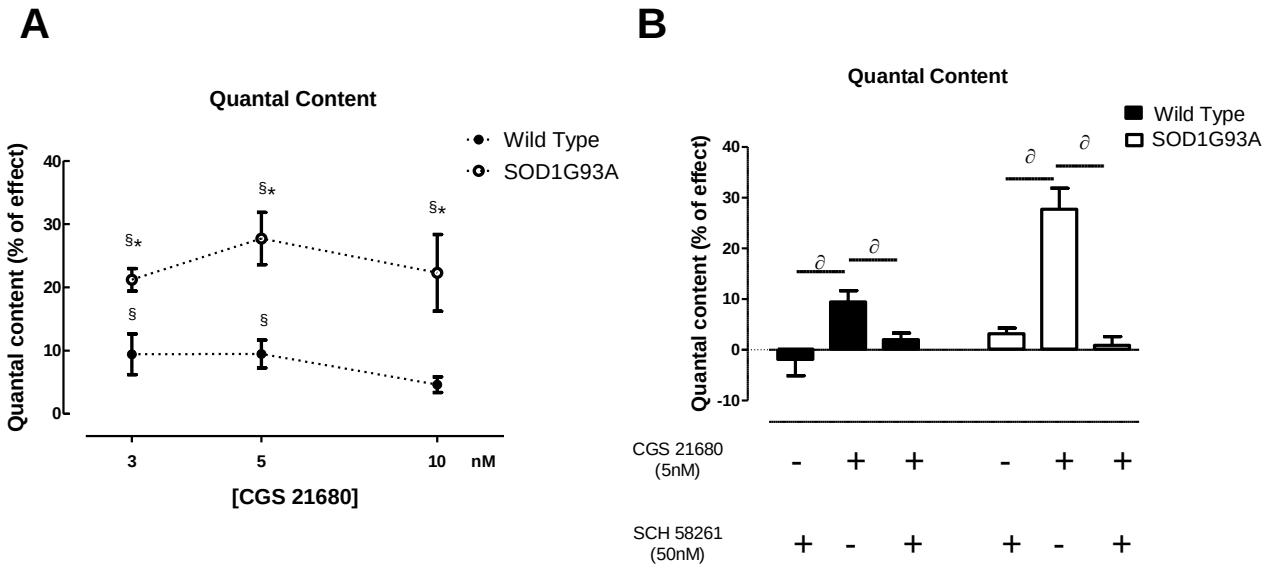

Figure 4.2.2 – **(A)** Variation in QC promoted by CGS 21680 in WT and SOD1G93A mice (3nM: n=5, WT, n=4, SOD1G93A; 5nM: n=8, WT, n=10, SOD1G93A; 10nM: n=4, WT, n=4, SOD1G93A); **(B)** bars elucidative of the A2AR blocking effect by SCH 58261 at 50 nM (SCH 58261 (50nM): n=4, WT,

n=5, SOD1G93A; CGS 21680 (5nM) in the presence of SCH 58261 (50nM): n=4, WT, n=6, SOD1G93A); § Paired *t*-test (as compared with mean QC before drug perfusion), ∂p<0.05 one-way ANOVA followed by Tukey's pos-hoc, *p<0.05 Unpaired *t*-test.

4.2.1.2. Spontaneous activity

MEPP amplitude was not significantly changed by the A2AR receptor selective agonist CGS 21680 in 4-6 wo animals (p>0.05 Paired *t*-test) (figure 4.2.3A). No significant differences were found between groups at 3 nM (0.15±2.58%, n=6, WT, 1.76±4.28%, n=5, SOD1G93A), 5 nM (1.29±1.98%, n=12, WT, 2.98±0.91%, n=12, SOD1G93A) and 10 nM (2.11±3.46%, n=7, WT, -2.17±2.18%, n=5, SOD1G93A) of CGS 21680 (p>0.05 Unpaired *t*-test).

SCH 58216 (50nM) did not statistically change MEPP amplitude (0.99±3.27%, n=5, WT; 1.45±1.75%, n=4, SOD1G93A; p>0.05 Paired *t*-test) and therefore no differences were found between different drug perfusions (p>0.05, one-way ANOVA) (figure 4.2.3B).

Figure 4.2.3C illustrates the effect of CGS 21680 in MEPP frequency. MEPP frequency was did not statistically change in WT (p>0.05 Paired t-test) as opposite of SOD1G93A mice (p<0.05 Paired *t-test).* At 3nM the A2AR-mediated increase in MEPP frequency did not significantly change between WT and SOD1G93A animals (14.55±7.26%, n=6, WT, 29.59±11.44%, n=5; p>0.05 Unpaired *t*-test). With 5 nM, SOD1G93A mice had significantly increased facilitation of MEPP frequency than WT mice (6.36±3.79%, n=12, WT, 23.13±7.03%, n=12, SOD1G93A; p<0.05 Unpaired *t*-test). CGS 21680 (10nM) effect on MEPP frequency was slightly lower in SOD1G93A (7.10±4.35%, n=7)

when compared to WT animals (26.87±12.13%, n=5) but this difference was not statistically different (p>0.05 Unpaired *t*-test).

To confirm that the effect of CGS 21680 was through A2AR activation, its action was evaluated in the presence of the A2AR selective antagonist, SCH 58261 (50nM). Alone, SCH 58261 did not change MEPP frequency in both groups of mice (2.40±2.29%, n=5, WT, 1.18±3.54%, n=4, SOD1G93A; p>0.05 Paired *t*-test). In the presence of the A2AR antagonist (SCH 58261) at 50 nM (figure 4.2.3D), the CGS 21680 (5nM) increase in MEPP frequency was abolished in SOD1G93A mice (-3.19±0.20%, n=3, p<0.05 one-way ANOVA followed by Tukey's pos-hoc) while in WT animals no differences were observed (-3.04±1.19%, n=4, p>0.05 one-way ANOVA). This suggests that A2AR act presynaptically by modifying the frequency of spontaneous release, which is in agreement to what was previously described [123].

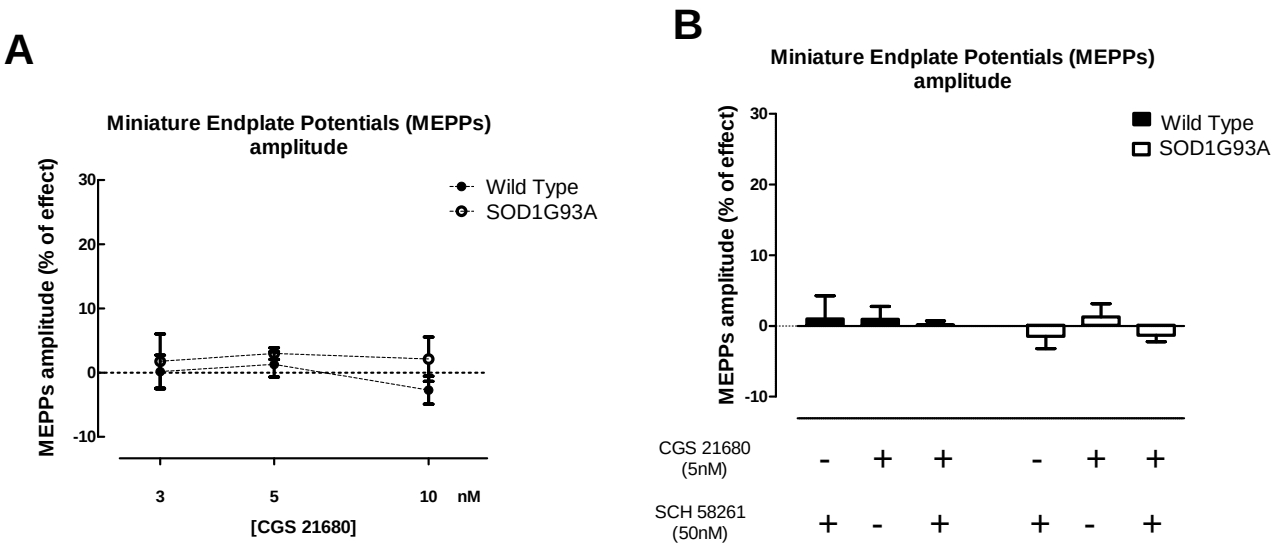

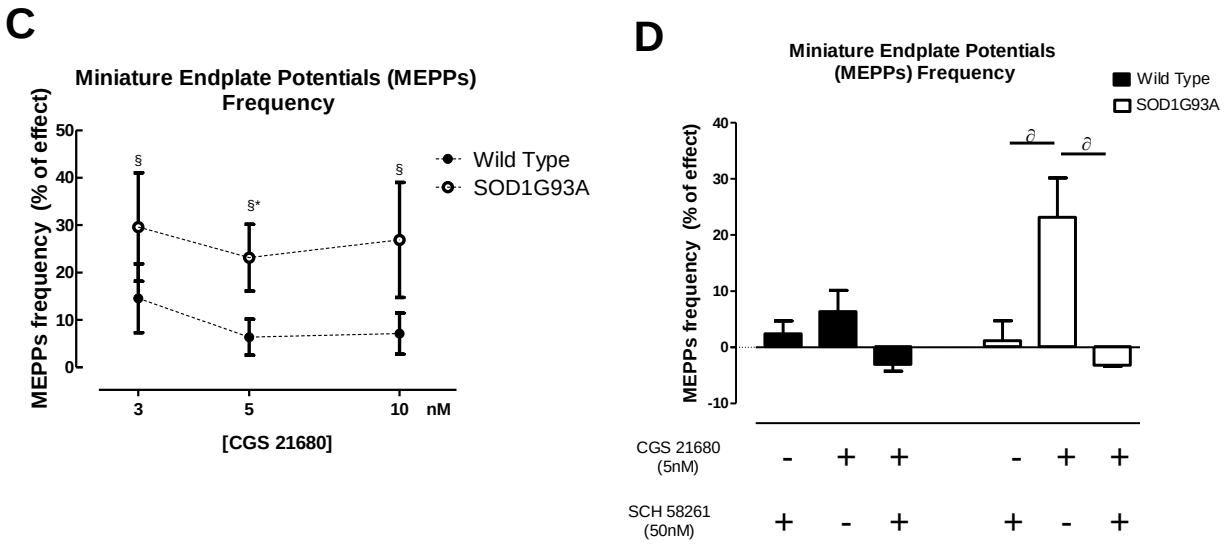

Figure 4.2.3 – **(A)** Effect of CGS 21680 at different concentrations in MEPP amplitude in WT and SOD1G93A mice (3nM: n=6, WT, n=5, SOD1G93A; 5nM: n=12, WT; n=12, SOD1G93A; 10nM: n=7, WT, n=5, SOD1G93A); **(B)** MEPP amplitude under the action of SCH 58261 (50 nM) (SCH 58261 (50nM): n=5, WT; n=4 SOD1G93A; CGS 21680 (5 nM) in the presence of SCH 58261 (50nM): n=4, WT, n=3, SOD1G93A); **(C)** changes in the MEPP frequency of both 4-6 wo WT and pre-symptomatic SOD1G93A animals promoted by CGS 21680 at 3 different concentrations (3, 5 and 10 nM) (3nM: n=6, WT, n=5, SOD1G93A; 5nM: n=12, WT; n=12, SOD1G93A; 10nM: n=7, WT, n=5, SOD1G93A); **(D)** SCH 58261 blocked the CGS 21680 increase in MEPP frequency (SCH 58261(50nM): n=5, WT, n=4, SOD1G93A; CGS 21680 (5nM) in the presence of SCH 58261 (50nM): n=4, WT, n=3, SOD1G93A); $^{\S}p<0.05$ Paired *t*-test as compared with MEPP frequency before adding the drug, $^{\partial}p<0.05$ one-way ANOVA followed by Tukey's pos-hoc, *p<0.05 Unpaired *t*-test.

Since GMEPPs were not very frequent, we could only analyze their amplitude and frequency when we tested 5nM of CGS21680 due to the higher number of experiments performed at that concentration. GMEPP amplitude remained unchanged upon A2AR activation (by CGS 21680 at 5 nM) (p>0.05 Paired *t*-test) (figure 4.2.4A). When we compared both WT (0.64±2.57%, n=3) and SOD1G93A (0.12± 5.74%, n=3) groups there was no statistical difference (p>0.05 Unpaired *t*-test). GMEPP frequency (figure 4.2.7B) was markedly increased in SOD1G93A (107.94±12.99%, n=3) when compared to WT mice (18.85±13.68%, n=3) (p<0.05 Unpaired *t*-test) (figure 4.2.4B).

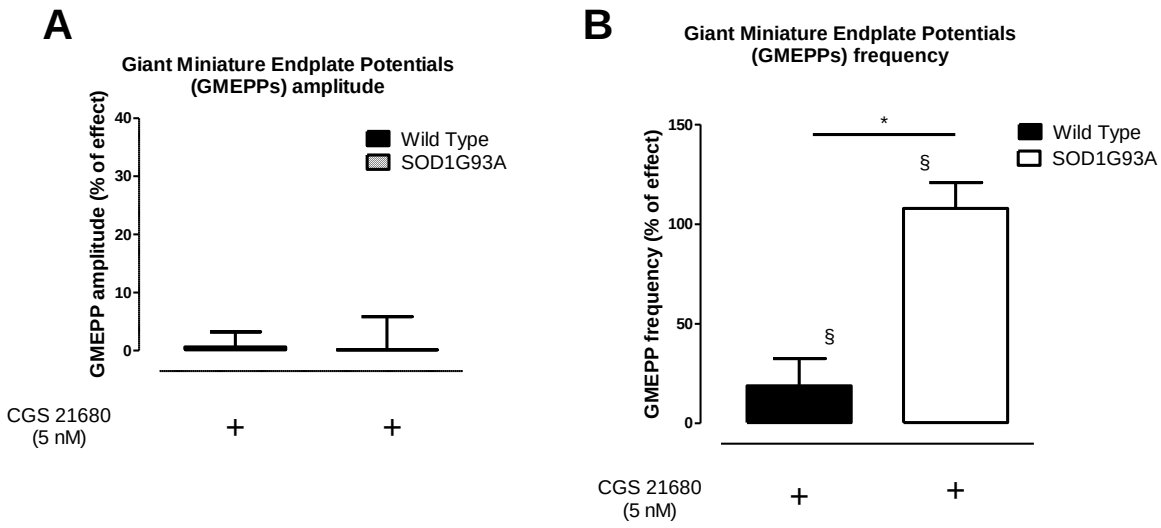

Figure 4.2.4 – **(A)** Effect of CGS 21680 (5nM) in GMEPP amplitude in 4-6 wo WT (n=3) and SOD1G93A (n=3) mice; **(B)** GMEPP frequency facilitation upon A2AR activation in both groups (n=3, WT, n=3, SOD1G93A); §p<0.05 Paired *t*-test as compared with GMEPP frequency before adding the drug; $^{\partial}$p<0.05 one-way ANOVA followed by Tukey's pos-hoc; *p<0.05 Unpaired *t*-test

4.2.2. Symptomatic phase

4.2.2.1. Evoked activity

In 12-14 wo WT animals we observed an increase in EPP amplitude in all tested of concentrations of CGS 21680 (3, 5, 10 and 25 nM), which was different from symptomatic SOD1G93A mice as follows: 3nM: 19.33±3.88% (n=8) in WT and -8.70±2.02 (n=9) in SOD1G93A mice; 5nM: 20.04±3.27% (n=7) in control mice and -6.44±5.20% (n=4) in symptomatic mice; 10nM: 24.60±6.92% (n=7) in WT and -2.38±3.14% (n=5) in ALS mice; 25nM: 11.75±1.15% (n=4) in 12-14 wo WT mice and -8.84±11.45% (n=4) in SOD1G93A rodents ($p<0.05$ Unpaired *t*-test) (figure 4.2.5A). Figure 4.2.5B evidences the different EPP amplitude changes in WT and SOD1G93A throughout CGS 21680 (5nM) perfusion.

Since in WT mice at 10nM we had a higher facilitation of EPP amplitude than in the other concentrations (but non-significant, $p>0.05$ one-way ANOVA), we tested the A2AR antagonist SCH 58261 (50nM) in the presence of the selective A2AR agonist (CGS 21680) to verify if the observed effect was through A2AR activation. SCH 58261 (50nM) blocked the CGS 21680 (10 nM) EPP amplitude increase in WT mice (-1.89±6.64%, n=3, $p<0.05$ one-way ANOVA following Tukey's pos-hoc). The A2AR antagonist did not display any effect in EPP amplitude in both WT (-0.24±2.41%, n=3) and SOD1G93A mice (-3.98±1.29%, n=6) ($p>0.05$ Paired *t*-test) (figure 4.2.5C).

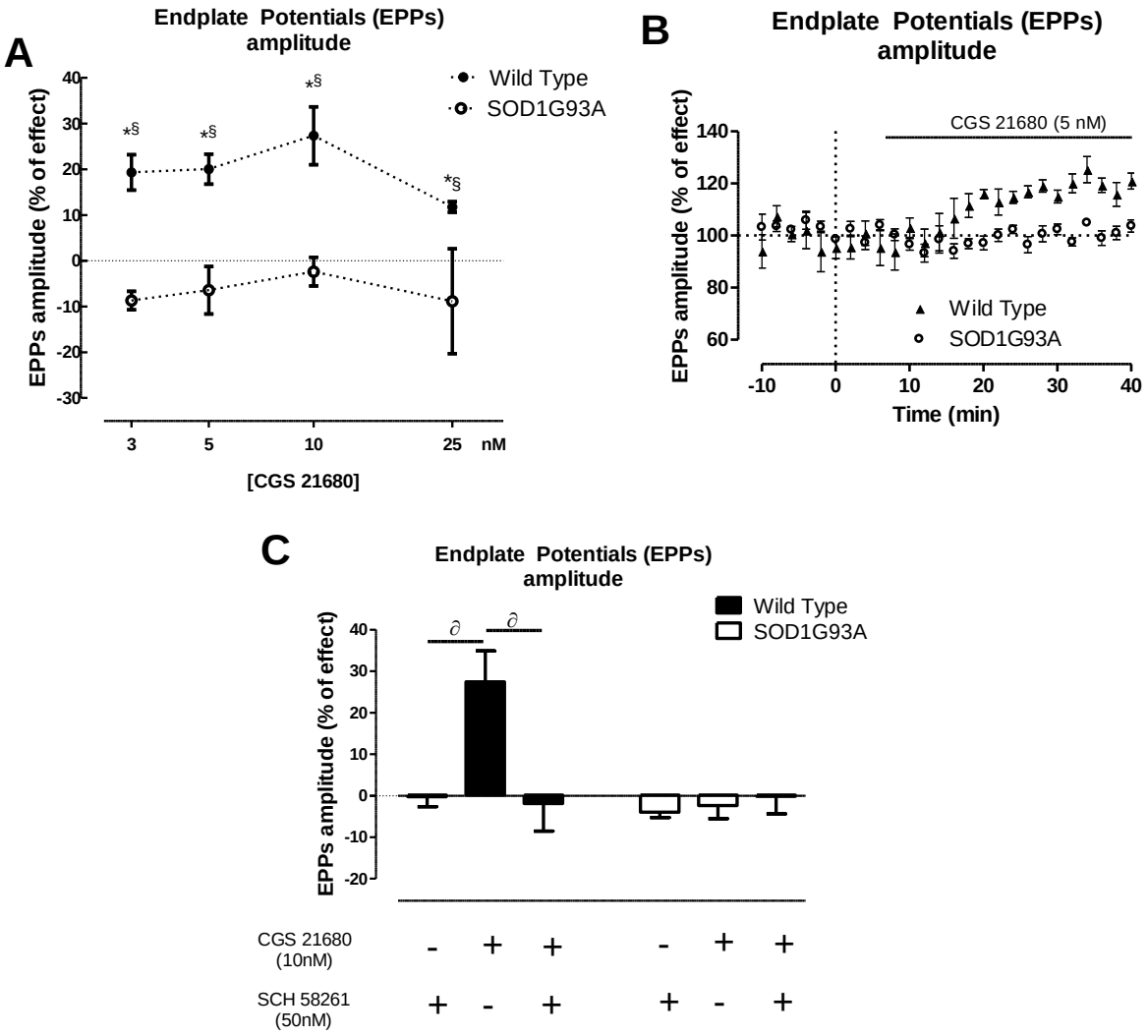

Figure 4.2.5 - **A)** percentage-change in EPP amplitude from 12-14 wo WT and symptomatic SOD1G93A animals after application of CGS 21680 (3 nM: n=8, WT, n=9, SOD1G93A; 5nM: n=7, WT, n=4, SOD1G93A; 10nM: n=7, WT, n=5, SOD1G93A; 25 nM: n=4, WT, n=4, SOD1G93A; **(B)** representative averaged changes in EPP amplitude in 12-14 wo and symptomatic mice mice upon A2AR activation by CGS21680 (5nM) (n=4, WT, n=4 SOD1G93A); **(C)** bar graph of CGS 21680 (10nM) effect in the presence of SCH 58261 (50nM) (SCH 58261 (50 nM): n=3, WT, - n=6, SOD1G93A; CGS 21680 (10nM) in the presence of SCH 58261 (50nM): n=3, WT; n=6, SOD1G93A); $^{\S}p<0.05$ Paired *t*-test as

compared mean EPP amplitude before adding the drug, $^{\partial}p<0.05$ one-way ANOVA followed by Tukey's pos-hoc, *p<0.05 Unpaired *t*-test.

When comparing QC change as a result of A2AR activation, we observed that QC was significantly increased in WT mice at 3 nM (17.54±6.31%, n=5, WT, -0.24±0.85%, n=5, SOD1G93A), 5 nM (17.56±2.55%, n=5, WT, 2.08±3.78%, n=4, SOD1G93A), 10 nM (29.91±5.88%, n=5, WT, -1.55±3.20%, n=3, SOD1G93A) and 25 nM of CGS 21680 (10.42±2.70%, n=4, WT, -9.45±9.98%, n=4) (p<0.05, Unpaired *t*-test) (figure 4.2.6A).

In figure 4.2.6B we can observe that the application of SCH 58261 at 50 nM blocked the CGS 21680 (10 nM) effect on the QC increase in WT mice (-5.02±4.85%, n=3, p<0.05 one-way ANOVA followed by Tukey's pos-hoc). The A2AR antagonist did not change the QC of both groups (5.07±2.79%, n=3, WT, 6.06±6.27%, n=3, SOD1G93A; p>0.05 Paired *t*-test).

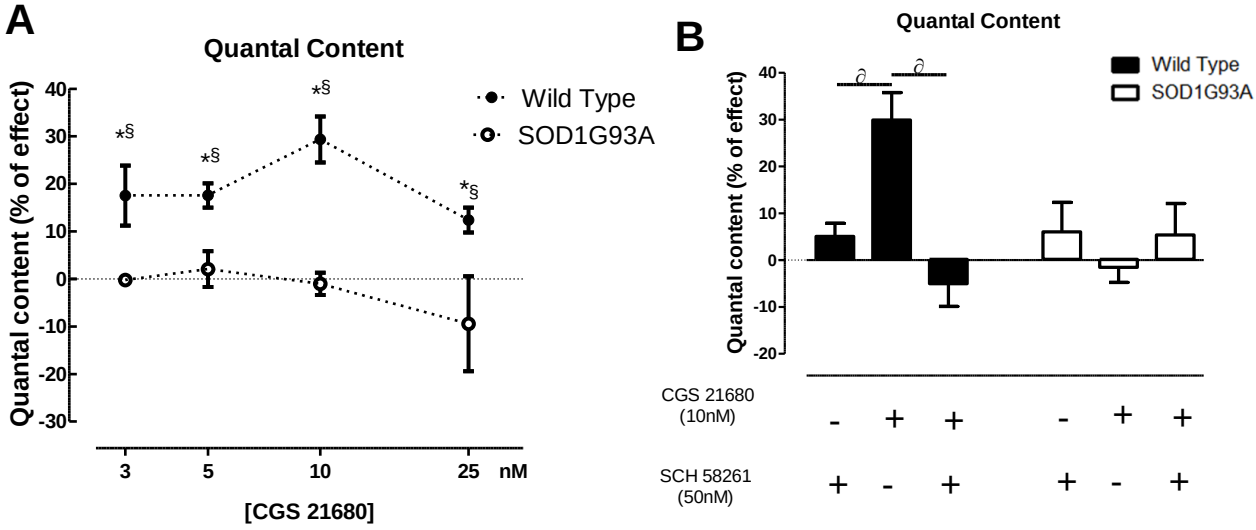

Figure 4.2.6 - **(A)** evidences a dose-response change in the QC of WT mice while in symptomatic mice CGS 21680 had no effect in QC (3 nM: n=5, WT, n=5, SOD1G93A; 5 nM: n=5, WT, n=4, SOD1G93A; 10 nM: n=5, WT, n=3,

SOD1G93A; 25nM: n=4, WT, n=4, SOD1G93A); **(B)** CGS 21680 (10 nM) effect in WT is blocked by SCH 58261 (50nM) (SCH (50nM): n=3, WT, n=3, SOD1G93A; CGS 21680 (10nM) in the presence of SCH 58261 (50nM): n=3, WT; n=3, SOD1G93A); $^{\S}p<0.05$ Paired *t*-test as compared with QC before addition of CGS 21680, $^{\partial}p<0.05$ one-way ANOVA followed by Tukey's pos-hoc, *p<0.05 Unpaired *t*-test.

4.2.2.2. Spontaneous activity

MEPP amplitude did not significantly change between groups in all tested concentrations of CGS 21680 (p>0.05 Paired *t*-test) and therefore no significant changes were found between groups (3nM: -1.84±1.61, n=5, WT, -5.63±3.52%, n=5, SOD1G93A; 5nM: 1.12±1.61%, n=5, WT, -5.81±2.54%, n=6, SOD1G93A; 10nM: 0.68±1.55%, n=6, WT, 1.05±5.60%, n=4, SOD1G93A; 25 nM: 1.50±2.54%, n=4, WT, -1.42±4.91%, n=4, SOD1G93A; p>0.05 Unpaired *t*-test) (figure 4.2.7A).

In Figure 4.2.7B we can observe that SCH 58261 (50nM) did not alter MEPP amplitude (p>0.05 Paired *t*-test) in 12-14 wo innervated muscle fibers (SCH 58261 (50nM): 0.61±0.81%, n=6, WT, -8.51±7.46%, n=3, SOD1G93A; CGS 21680 (10nM) in the presence of SCH 58261 (50nM): 0.61±0.81%, n=5, WT, -8.51±7.46, n=3, SOD1G93A).

When perfusing 3nM of CGS 21680, MEPP frequency was 17.04±3.62% (n=5) increased in WT mice, it was significantly higher than in SOD1G93A mice (-0.27±3.60%, n=5) (p<0.05 Unpaired *t*-test). MEPP frequency was also significantly higher in WT mice at 5nM (24.31±3.60%, n=5, WT, -1.30±5.23%, n=6, SOD1G93A) and 10 nM of CGS 21680 (19.49±5.04%, n=6, WT, -

3.46±7.78, n=4, SOD1G93A) ($p<0.05$ Unpaired *t*-test) (figure 4.2.7C). When using 25 nM, WT had an increase of 10.58±5.38% (n=4) significantly different from SOD1G93A mice (-16.00±10.27%, n=4) ($p<0.05$ Unpaired *t*-test). CGS 21680 was devoid of effect in symptomatic mice ($p>0.05$ Paired *t*-test).

In the presence of the A2AR antagonist SCH 58261 (50nM), the increase in MEPP frequency by CGS 21680 (10 nM) in WT mice was abolished (-0.14±5.47%, n=4; $p<0.05$ one-way ANOVA followed by Tukey's pos-hoc). SCH 58261 did not promote any effect in MEPP frequency in both WT (-0.12±1.57, n=5) and SOD1G93A (-0.10±17.42, n=4) animals ($p>0.05$ Paired *t*-test) (figure 4.2.7D).

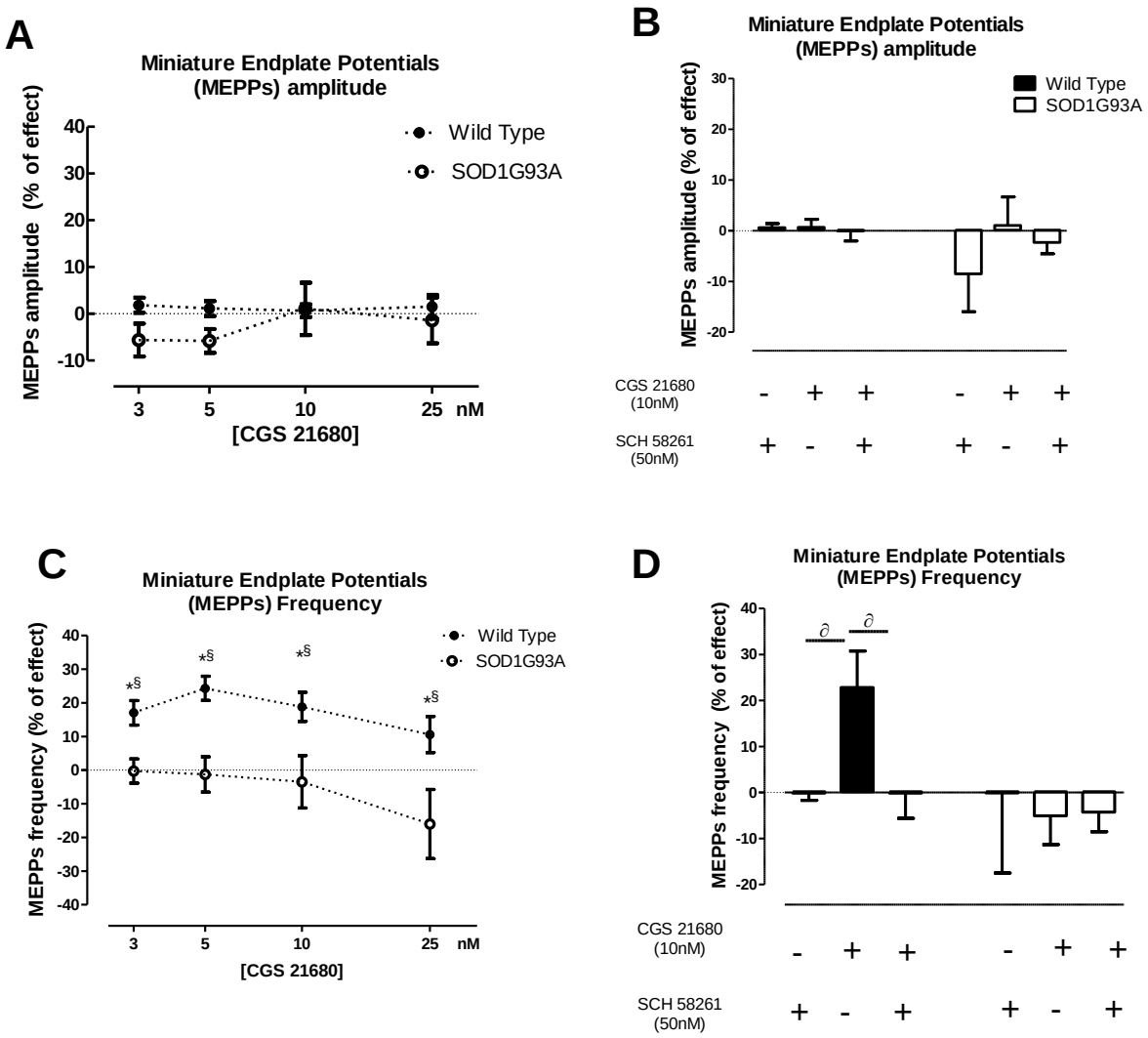

Figure 4.2.7 – **(A)** graphic representation evidencing no changes in MEPP amplitude after A2AR activation by CGS 21680 (3nM: n=5, WT, n=5, SOD1G93A; 5nM: n=5, WT, n=6, SOD1G93A; 10nM: n=6, WT, n=4, SOD1G93A; 25 nM: n=4, WT, n=4, SOD1G93A); **(B)** effect of CGS 21680 (10nM), SCH 58261 (50nM) and both drugs applied (SCH 58261 (50nM): n=6, WT, , n=3, SOD1G93A; CGS 21680 (10nM) in the presence of SCH 58261 (50nM): n=5, WT, n=3, SOD1G93A); **(C)** excitatory concentration-dependent effect of CGS 21680 in MEPP frequency of WT and null effect in symptomatic SOD1G93A mice (3nM: n=5, WT, n=5, SOD1G93A; 5nM: n=5, WT, n=6, SOD1G93A; 10nM: n=6, WT, n=4, SOD1G93A; 25nM: n=4, WT, n=4, SOD1G93A); **(D)** SCH 58261 (50nM) effectively blocked MEPP frequency increase by 10 nM of the A2AR agonist in 12-14 wo WT rodents (SCH 58261 (50nM): n=5, WT, n=4, SOD1G93A; CGS 21680 (10nM) in the presence of 50nM of SCH 58261: n=4, WT, n=4, SOD1G93A); $^{\S}p<0.05$ Paired *t*-test as compared with control MEPP frequency before drug perfusion, $^{\partial}p<0.05$ one-way ANOVA followed by Tukey's pos-hoc, *p<0.05 Unpaired *t*-test.

GMEPP amplitude was not significantly changed by CGS21680 (10nM) in both WT (3.04±1.47%, n=3) and SOD1G93A animals (-2.27±6.69%, n=3) (figure 4.2.8A) (p>0.05 Paired *t*-test). GMEPP frequency was statistically increased in WT when compared to symptomatic ALS mice in the presence of 10nM of the A2AR agonist (73.87±19.43%, n=3, WT, 10.16±17.60%, n=3, SOD1G93A; p<0.05 Unpaired *t*-test) (figure 4.2.8B).

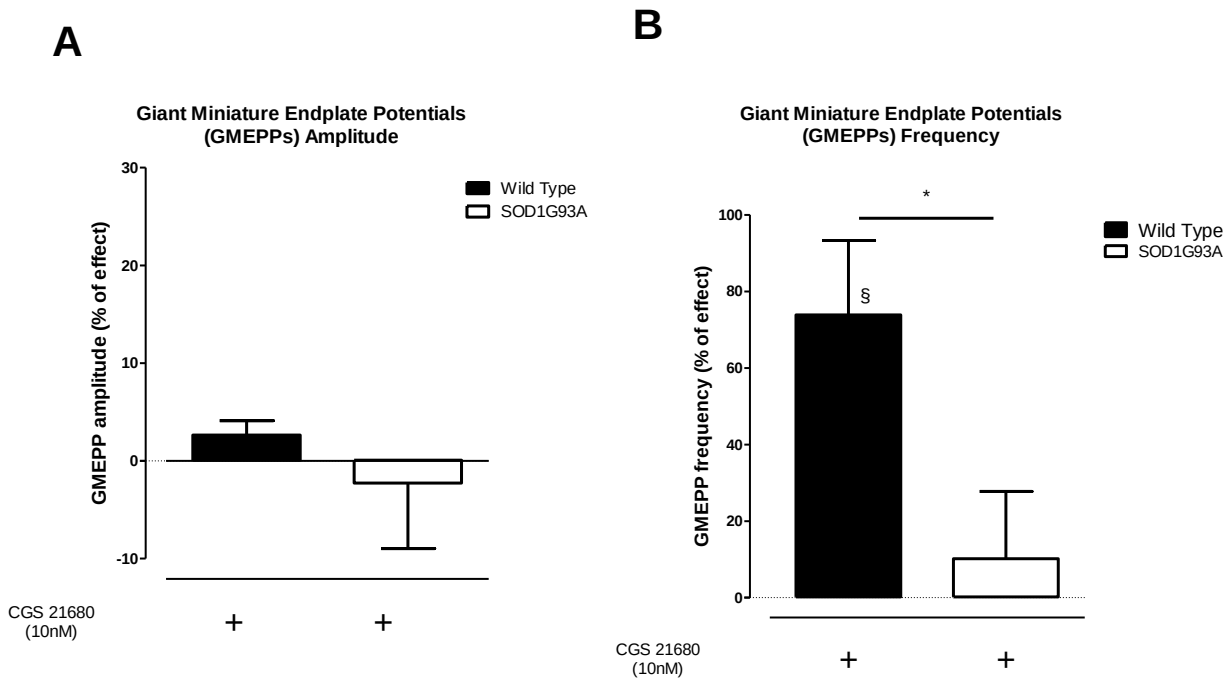

Figure 4.2.8 – **(A)** bar-chart representation of GMEPP amplitude change by CGS 21680 (10nM) (n=3, WT, n=3, SOD1G93A); **(B)** GMEPP frequency variation in the presence of 10nM of CGS 21680 (n=3, WT, n=3, SOD1G93A); $^{\S}p<0.05$ Paired *t*-test as compared with GMEPP frequency before start perfusion; $^{\partial}p<0.05$ one-way ANOVA followed by Tukey's pos-hoc;*p<0.05 Unpaired *t*-test

4.2.3. Comparison between phases

4.2.3.1. Evoked activity

Regarding WT animals, the selective A2AR agonist caused a more pronounced excitatory effect in EPP amplitude in older WT (12-14 wo) than in younger WT (4-6 wo) animals. This increment was evident at 3, 5 and 10nM of CGS 21680 (figure 4.2.9A) (p>0.05 Unpaired *t*-test). Comparison of EPP

amplitude changes between 5nM of A2AR agonist perfusion in 4-6 wo and 12-14 wo WT can be observed in figure 4.2.9B.

An opposite situation occurred in SOD1G93A animals. In pre-symptomatic ALS mice, CGS 21680 had an excitatory effect in EPP amplitude at 3, 5 and 10nM (figure 4.2.9C) but when symptoms started to appear, the A2AR agonist did not modify the evoked activity of SOD1G93A mice ($p<0.05$ Unpaired *t*-test). This is clearly illustrated in figure 4.2.9D.

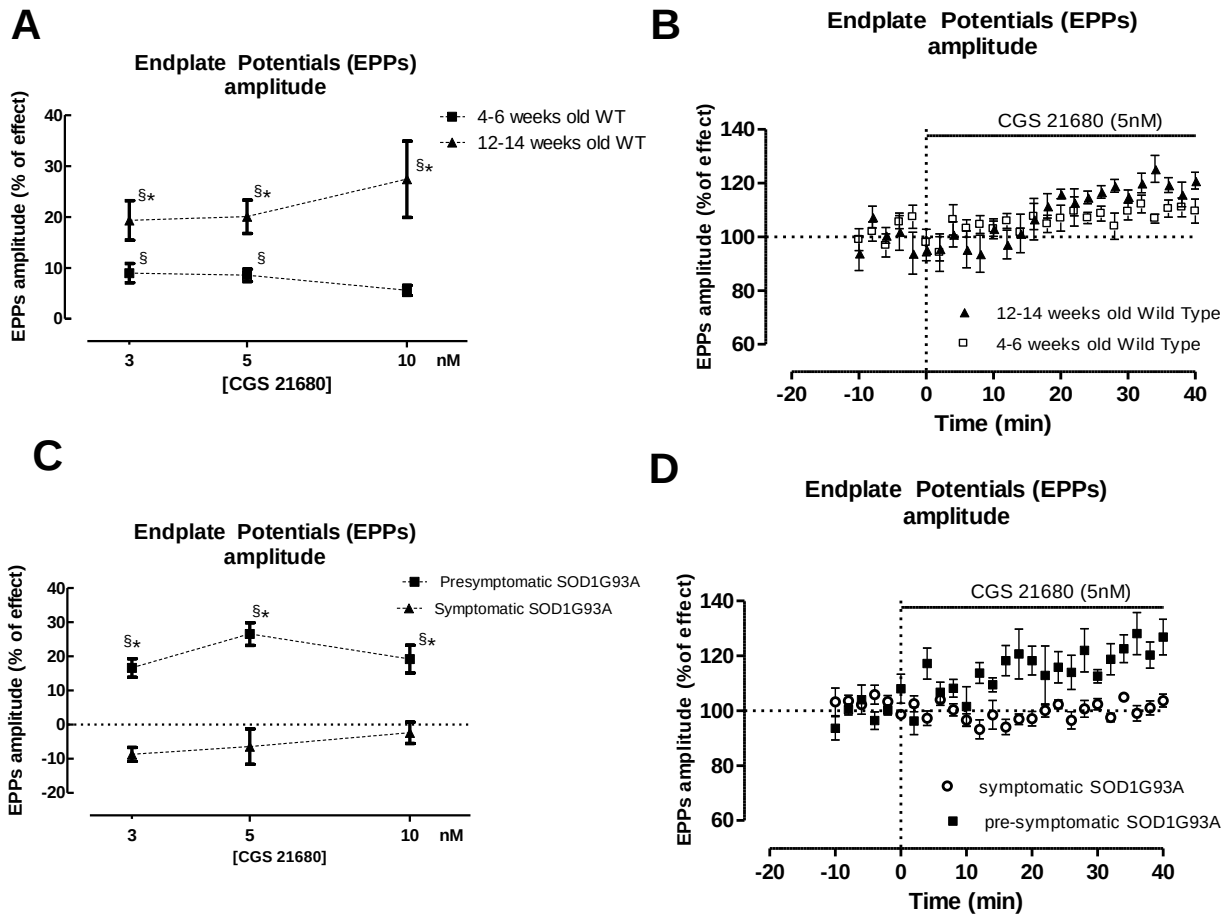

Figure 4.2. 9 – **(A)** changes in EPP amplitude promoted by CGS 21680 (3, 5 and 10 nM) in different aged WT animals (4-6 wo WT: 3nM, n=7, 5nM, n=8, 10nM, n= 4; 12-14 wo WT: 3nM, n=8, 5nM, n=7, 10nM, n=7); **(B)** representation of the EPPs changes (CGS 21680 at 5 nM) in 4-6 wo (n=4) and 12-14 wo mice (n=4); **(C)** Symptomatic SOD1G93A mice lose their A2AR facilitation when

symptoms start to arise (pre-symptomatic SOD1G93A: 3nM, n=5, 5nM, n=15, 10nM, n=5; symptomatic SOD1G93A: 3nM, n=9, 5nM, n=4, 10 nM, n=5); **(D)** Averaged changes in EPP amplitude in the presence of CGS 21680 and in the different stages of disease progression in SOD1G93A mice (n=6, pre-symptomatic SOD1G93A; n=4, symptomatic SOD1G93A); $^{\S}p<0.05$ Paired *t*-test as compared with mean EPP amplitude before starting drug perfusion,*p<0.05 Unpaired *t*-test

The QC exhibits the same pattern of changes as EPP amplitude when comparing the different stages in both groups of animals (figure 4.2.10). A shift in effective concentrations of CGS 21680 effect seemed to occur. In 4-6 wo WT, 10 nM of the A2AR agonist did not promote a statistical significant increase of QC while in older animals (12-14 wo), at this concentration, the facilitation was apparently maximum (but non-statistically significant, p>0.05 one-way ANOVA).

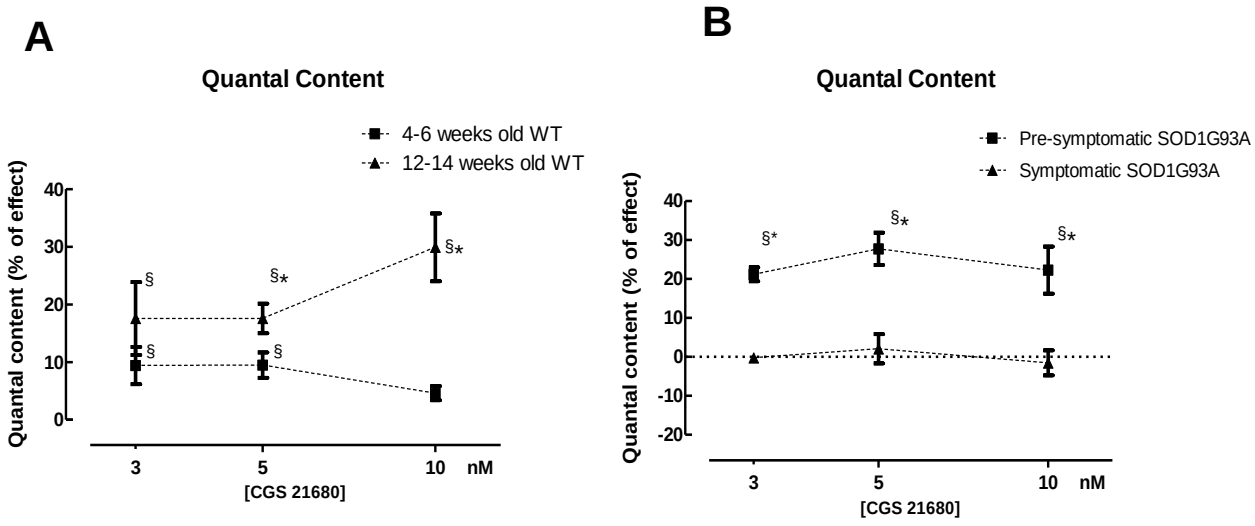

Figure 4.2.10 – **(A)** An increase in QC facilitation is evident when comparing 12-14 wo with 4-6 wo WT mice (4-6 wo WT: 3nM, n=5, 5nM, n=8, 10nM, n= 4; 12-14 wo WT: 3nM, n=5, 5nM, n=5, 10nM, n=5; **(B)** QC is not affected by A2AR

activation in all tested concentrations of CGS 21680 when symptomatology arises in SOD1G93A animals (pre-symptomatic SOD1G93A: 3nM, n=4, 5nM, n=10, 10nM, n=4; symptomatic SOD1G93A: 3nM, n=5, 5nM, n=4, 10 nM, n=3); $^{\S}p<0.05$ Paired *t*-test as compared with QC before drug perfusion;*p<0.05 Unpaired *t*-test

4.2.3.2. Spontaneous activity

MEPP amplitude was not altered by A2AR activation in WT and SOD1G93A animals (p>0.05 Paired *t*-test). MEPP frequency did not vary between ages in WT animals at 3 and 10 nM of CGS 21680, but at 5nM it was significantly increased in older (12-14 wo) WT animals (p<0.05 Unpaired *t*-test). In SOD1G93A mice, the pre-symptomatic CGS 21680-mediated increase in MEPP frequency was lost in the symptomatic stage (p<0.05 Unpaired *t*-test) (see figure 4.2.11).

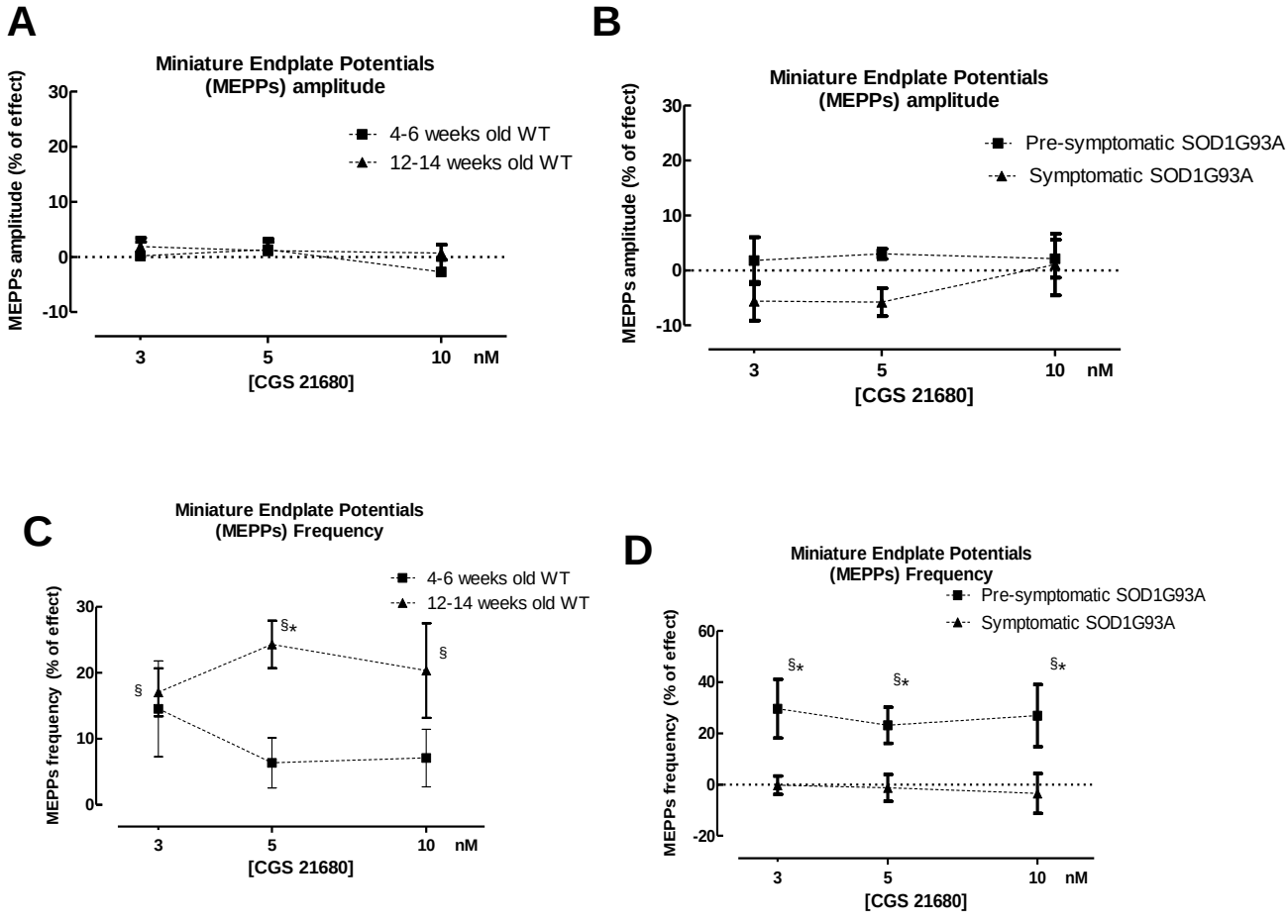

Figure 4.2.11- **(A)** MEPP amplitude does not change in WT animals (4-6 wo WT: 3nM, n=6, 5nM, n=12, 10nM, n= 7; 12-14 wo WT: 3nM, n=5, 5nM, n=5, 10nM, n=6) and **(B)** SOD1G93A mice (pre-symptomatic SOD1G93A: 3nM, n=5, 5nM, n=12, 10nM, n=5; symptomatic SOD1G93A: 3nM, n=5, 5nM, n=6, 10 nM, n=4), due to A2AR activation by CGS 21680; **(C)** MEPP frequency changes in WT animals (4-6 wo WT: 3nM, n=6, 5nM, n=12, 10nM, n= 7; 12-14 wo WT: 3nM, n=5, 5nM, n=5, 10nM, n=6) and **(D)** pre-symptomatic and symptomatic SOD1G93A(pre-symptomatic SOD1G93A: 3nM, n=5, 5nM, n=12, 10nM, n=5; symptomatic SOD1G93A: 3nM, n=5, 5nM, n=6, 10 nM, n=4) in the presence of the referred concentrations of CGS 21680; $^{\S}p<0.05$ Paired *t*-test as compared with control MEPP frequency before drug perfusion;*p<0.05 Unpaired *t*-test

GMEPP amplitude was not changed by CGS 21680 in both SOD1G93A and WT groups (p>0.05 Paired *t*-test) (figure 4.2.12A). Regarding GMEPP frequency, in WT mice it was statistically increased in 12-14 wo animals when compared to 4-6 wo rodents (p<0.05 Unpaired *t*-test). This comparison was made between different concentrations of CGS 21680 (5nM in 4-6 wo mice and 10nM in 12-14 wo rodents) that elicited increases in GMEPP frequency. In SOD1G93A, the raise in GMEPP frequency in the pre-symptomatic stage (CGS 21680 at 5nM), was lost in symptomatic SOD1G93A mice (CGS 21680 at 10 nM) (p<0.05 Unpaired *t*-test) (see figure 4.2.12B).

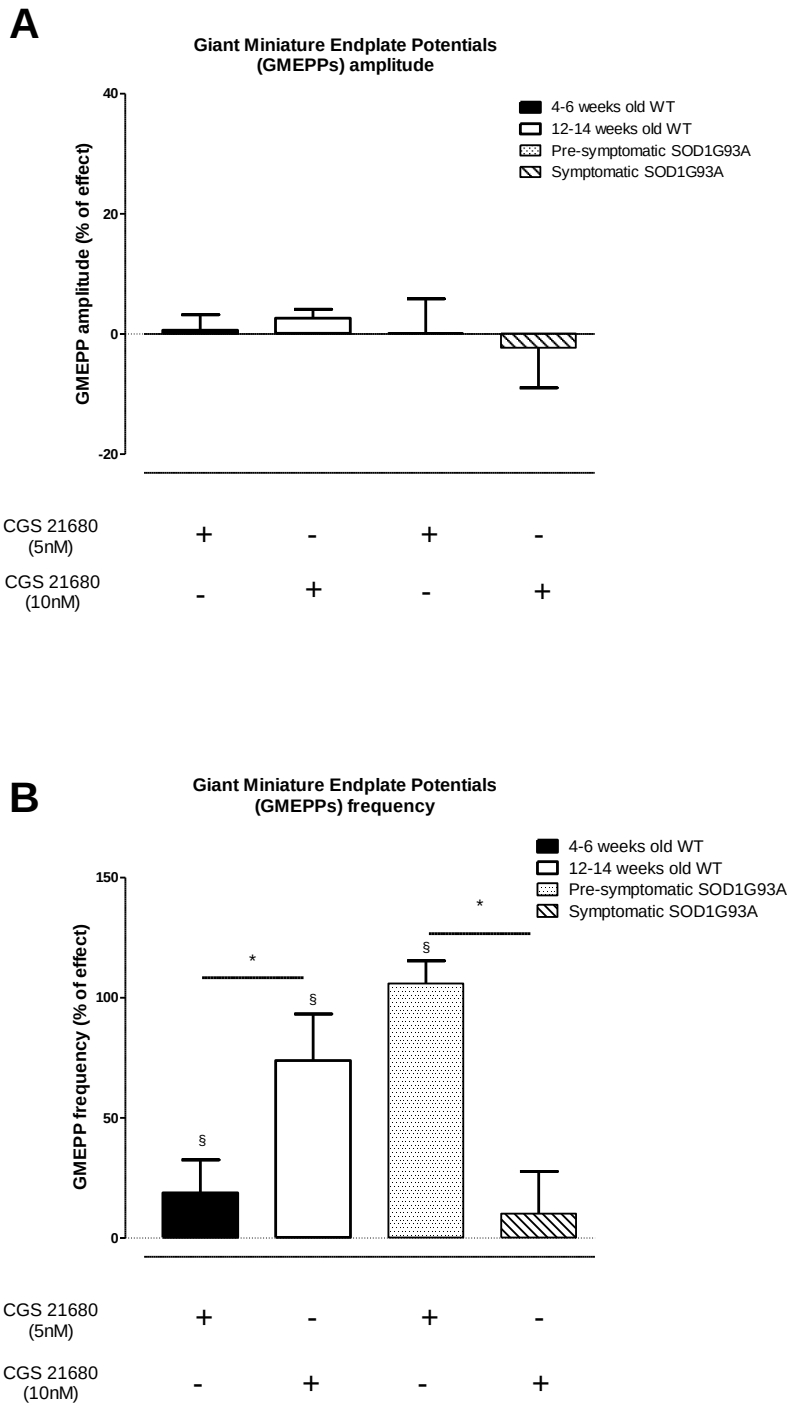

Figure 4.2.12 – (A) A2AR activation effect in GMEPP amplitude in the different phases of the disease at the different concentrations of CGS 21680 used (5nM in younger animals (4-6 wo) and 10 nM in 12-14 wo mice) (5nM: n=3, 4-6 wo WT, n=3, pre-symptomatic SOD1G93A; 10nM: n=3, 12-14 wo WT, n=3, symptomatic SOD1G93A); **(B)** GMEPP frequency was increased in 12-14 wo

WT mice when compared to 4-6 wo WT rodents, and the opposite is observed in SOD1G93A mice where the GMEPP frequency increase in pre-symptomatic animals is lost along disease progression in the presence of the A2AR agonist (5nM: n=3, 4-6 wo WT, n=3, pre-symptomatic SOD1G93A; 10nM: n=3, 12-14 wo WT, n=3, symptomatic SOD1G93A); $p<0.05$ Paired *t*-test as compared with GMEPP frequency before drug perfusion, $*p<0.05$ Unpaired *t*-test

5. Discussion

The results herein described clearly showed that, in the presence of high [Mg^{2+}] and low frequency stimulation (0.5 Hz), the effects of A2AR are enhanced in phrenic nerve-hemidiaphragm preparations from pre-symptomatic SOD1G93A mice an ALS transgenic model. On the contrary, in the symptomatic phase the A2AR effect was lost.

5.1. Principal features of the neuromuscular transmission in SOD1G93A mice are maintained in the presence of high [Mg^{2+}]

It is well-known that increase in [Mg^{2+}] to avoid muscle fiber contraction in intracellular recordings, decreases EPP amplitude and QC [114]. Fine-tuning of [Mg^{2+}] in both studied phases of disease progression was done to allow electrophysiology recordings, and therefore evoked activity parameters strongly deviated from physiologic values [31]. Differences in EPP (only in SOD1G93A) and QC when comparing the same group at different ages are evidence of NMJ maturation, which is an intrinsic feature in the NMT of these animals. Increased MEPP frequency in 12-14 wo WT in comparison to 4-6 wo WT mice also supports this idea. Decreased MEPP amplitude and area in symptomatic mice in contrast with pre-symptomatic animals, highlighted the neurodegenerative events affecting spontaneous ACh release at the NMJ throughout disease progression [31].

Regarding pre-symptomatic and age matched WT mice comparisons, increased MEPP amplitude and GMEPP amplitude and frequency in pre-symptomatic rodents are evidence of the increased spontaneous NMT features

of the SOD1G93A animal model. When symptomatology arises, MEPP frequency, amplitude and area are decreased in SOD1G93A animals by contrast with 12-14 wo WT mice. This emphasized the intrinsic impairment regarding spontaneous release that symptomatic SOD1G93A mice display [31]. It is evident in our work that by using high [Mg^{2+}] to avoid muscle contraction, the main features of NMT in SOD1G93A phrenic nerve-hemidiaphragm preparations are preserved. This strategy is therefore an useful tool to study adenosinergic modulation at the SOD1G93A NMJ.

5.2. A_{2A} adenosine receptors are functionally up-regulated in pre-symptomatic SOD1G93A neuromuscular junctions

QC and EPP amplitude were significantly increased in pre-symptomatic SOD1G93A mice when A2AR were activated. Previous work evidenced a possible physiological compensatory mechanism leading to increased NMT in pre-symptomatic SOD1G93A mice [31]. A2AR are important modulators of NMT and upon activation can lead to an increase of ACh release. Since SCH 58261 (50nM) did not evidence any change in evoked activity, A2AR are not being tonically activated in young mice (4-6 wo). In infant rats, A2AR exhibit excitatory predominance over A1R inhibitory action [96]. However mice have a different physiology in diaphragmatic fibers when comparing to rats. Failures are less frequent in mice probably due to a higher proportion of fatigue-resistance fibers representative of total muscle diaphragm mass [124]. Since these types of fibers are less prone to degeneration in ALS [41], this physiological feature may account for an unnecessary constitutive A2AR activation. However, during high

frequency stimulation (50Hz) A2AR activation may be important for facilitation of ACh release [91]. ALS renders individuals susceptible to tetanic stimuli in a gender unspecific manner [125], and therefore A2AR upregulation could be a compensatory mechanism to overcome tetanic fade.

Adenosine is important in synchronizing transmitter release in oxidative stress conditions at the NMJ, therefore enhancing synaptic efficiency. SOD1G93A present high levels of reactive oxygen species, and therefore A2AR upregulation could account for a compensatory mechanism [126]. In fact administration of A2AR agonist CGS 21680 promoted MN survival [127] and delayed disease onset [103]. A2AR can promote the recruitment of L-type VGCC during repetitive stimulation [91]. In ALS IgGs immunoreactivity renders L-type VGCC sensitive to stimuli [88]. Therefore A2AR facilitation via L-type VGCC recruitment may be responsible for the observed functional upregulation in evoked activity probably by core-vesicle mobilization at the NMJ (see [128]). This subtype of VGCC is important in establishing Ca^{2+} micro and nano-domains. In SOD1G93A mice there is an increase in intra-terminal [Ca^{2+}] probability due to mitochondrial complex dysfunction (see [59]) but also to L-type VGCC increased recruitment [88]. Use of nitrendipine [L-type VGCC blocker] could be a future task towards unveiling this interaction.

Other types of VGCC have been implicated with ALS pathogenesis. N-type VGCC are overexpressed in the motor cortex neurons of SOD1G93A mice [129] and are modified by ALS sera together with L-type VGCC leading to increased MEPP frequency [130]. The same is observed regarding P/Q type-VGCC [131]. Yet, more emphasis is given to L-type channel dysfunction in ALS

[88, 129-130, 132]. These channels possess a longer length of activation leading to a higher intraterminal influx of Ca^{2+}. Therefore recruitment of these long-lasting channels could account for a compensatory mechanism in order to sustain NMT and result in increased concentration of the divalent ion at NMJs. However this could also contribute to the typical Ca^{2+} toxicity in ALS. Since L-type VGCCs are important in presynaptic autofacilitation of ACh release [133] and have an A2AR-mediated recruitment in high frequency stimuli [91], pre-symptomatic SOD1G93A mice upregulation of A2AR could contribute to the neurodegenerative mechanisms occurring at transgenic NMJs.

Spontaneous events arise from intracellular Ca^{2+} store mobilization upon RyRs activation, and are independent of extracellular Ca^{2+} levels [102]. CGS 21680 at tested concentrations (3, 5 and 10 nM) only increased the frequency of the spontaneous events (MEPPs and GMEPPs) highlighting the presynaptic action of A2AR [123].

It has been show that IgGs from sporadic ALS patients can lead to higher frequency of spontaneous events in mice phrenic nerve-hemidiaphragm preparations through Ca^{2+} influx from N-type VGCCs and PLC recruitment with RyR and IP_3 receptors being needed to sustain this feature [101]. A2AR activation results in increased spontaneous release through direct stimulation of ryanodine sensitive stores, while in K^+-evoked conditions A2AR signalization positively modulates L-type VGCC which may induce the opening of RyRs by increasing gating charge movements [102]. Pre-symptomatic terminals are more competent in handling activity-dependent Ca^{2+} load at moderate firing frequencies, but distinct mechanisms become apparent in maximal stimulation

resulting in higher peak Ca^{2+} amplitudes [63]. The different A2AR regulation of MEPP frequency in pre-symptomatic SOD1G93A fibers could be related with: (1) increased A2AR signaling leading to an uncontrolled resting intraterminal [Ca^{2+}] which could underlie the noticed changes in spontaneous release; (2) a deficient regulation of Ca^{2+} intracellular stores mechanisms that control Ca^{2+} clearance and limit the duration of the EPP [63], resulting in higher MEPP frequency upon A2AR activation; or (3) abnormal RyR Ca^{2+}-sensitization [134] resulting in A2AR promoted Ca^{2+}-induced Ca^{2+}-release from the ER explainable of observed results (see[135]) This mechanism could play a major role during high frequency bursts. But these hypotheses need further investigation.

In SOD1G93A muscle strength is lost and denervation starts before symptoms onset [41]. Muscle strength depends on the firing frequency and motor unit recruitment [136]. Pre-junctional changes in [Ca^{2+}] homeostasis may induce adaptations to facilitate firing frequency, specifically during high-frequency stimulation [128]. An increase in intraterminal [Ca^{2+}] could be derived from A2AR recruitment of VGCCs via PKA [137]. This may lead to higher nicotinic autofacilitation via α3β2 nAChR or higher intracellular store mobilization of Ca^{2+} attributable to pre-symptomatic pro-inflamatory factors present in SOD1G93A mice such as IgGs [138].

GMEPP frequency increase in pre-symptomatic mice is suggestive of enhanced synchronism in vesicle release, and highlights the role of A2AR in the facilitation of synchronous spontaneous release. GMEPP are also more present in pathological conditions, during reinervation processes and ageing [139-140] (but see[141]). Presynaptic terminal arrangement of ACh vesicles in

SOD1G93A may predispose to higher GMEPP frequency in the presence of CGS 21680 (5nM). Changes in resting intra-terminal [Ca^{2+}] concentration by mechanisms of Ca^{2+} influx, pointed before, may also trigger an increase in basal [Ca^{2+}] resulting in higher spontaneous synchronous release [140].

5.3. A_{2A} adenosine receptors modulation of acetylcholine release is lost in symptomatic SOD1G93A mice

Evoked activity (EPP amplitude and QC) in symptomatic mice is not changed by CGS 21680 (3, 5, 10 and 25nM) perfusion, contrasting with the effect of the A2AR agonist in WT mice. Symptomatic SOD1G93A display a reduced expression of A2AR in the spinal cord, a decrease that is mimicked in age-matched WT mice by chronic administration of caffeine (non-selective adenosine receptor antagonist) [104].

It is known that A2AR may decrease nicotinic autofaciltiation by favouring autodesensitisation of α3β2 nAChR at high-stimulated NMJs, perhaps to prevent ACh flooding and Ca^{2+} excitotoxicity [142]. With a high intraterminal [Ca^{2+}] VGCC recruitment could be decreased, like in other neuromuscular diseases such as myasthenia gravis where an abnormal A2AR interaction with L-type VGCC renders rat NMJs susceptible to tetanic failure [143]. The C-terminus of the L-type VGCC has a regulatory Ca^{2+} dependent inactivation and activation. This channel is also controlled by calmodulin, a Ca^{2+} binding messenger protein (see[144]). Calmodulin can interact with the A2AR structure producing conformational changes and shifts in signaling, a feature present in A2AR and dopamine D2 receptors heteromers [145]. Pre-symptomatic SOD1G93A Ca^{2+} transient hyperexcitability is lost when symptoms arise, and

Ca^{2+} overload at the MN terminal determines cell death due to deficient Ca^{2+} clearance [63]. In symptomatic SOD1G93A mice Ca^{2+} dysfunction may affect A2AR functionality resulting in cellular changes that impair the evoked excitatory adenosinergic action.

A picture of contrast can be observed between both WT and SOD1G93A mice at the different studied ages. In WT there was an increase in evoked activity in 12-14 wo mice when comparing with 4-6 wo animals, along with a shift in the concentration of the A2AR agonist concentration that can elicit the maximum effect in ACh facilitation (3-5nM in 4-6 wo WT and 10 nM in 12-14 wo), however non-significant. SOD1G93A presented an opposite feature. WT mice may undergo synapse maturation while SOD1G93A compensatory mechanisms may lead to a typical ALS-hyperexcitability envolving an A2AR functional enhancement at the NMJ. When symptoms arise A2AR modulation is lost in transgenic mice probability due to denervation processes, deficient signaling or as means to avoid Ca^{2+} excitotoxicity. Therefore A2AR functional downregulation could be a protective endstage mechanism to delay MN death.

In rat hemidiapragm, muscle paralysis by μ-conotoxin GIIIB decreased nerve evoked adenosine outflow around 90% [143]. In high-frequency stimulation a higher amount of adenosine may come from ATP breakdown which can then be uptaken by an adenosine sensitive transporter in rat skeletal muscle [146]. This may indicate that at our stimulus paradigm most of endogenous adenosine might come from the muscle fiber. Given the neurodegenerative events in ALS muscle, and since extracellular adenosine levels can be elevated in pathological conditions (see [93]), increased

extracellular adenosine levels might be present in symptomatic SOD1G93A mice resulting in an ablation of A2AR functionality. If adenosine is increased in the synaptic clef of transgenic animals, A2AR are not tonically activated since SCH 58261 (50nM) did not change EPP amplitude nor QC. Therefore perfusion of adenosine deaminase in phrenic nerve-hemidiaphragm preparations in the presence of the A2AR agonist could clarify this hypothesis.

NMJ alterations in old mice parallel with the observations in symptomatic SOD1G93A mice [147]. In ageing, a shift from fast towards slow twitch fibers is observed [148-149] involving purinergic modulation through adenine nucleotide release by the skeletal muscle [150]. Considering that early denervation occurs in ALS mice muscle with a fast to slow fiber transition, this may also contribute to changes in A2AR modulation.

Regarding spontaneous activity there was no change in MEPP frequency in symptomatic SOD1G93A rodents. One feature of ALS is the ER-stress that starts in the pre-symptomatic phase, and increases throughout disease progression. Mitochrondrial dysfunction, proteossome impairment and deficient cellular signaling are typical features of ER-stress (see [151]). Therefore A2AR action on intracellular Ca^{2+} stores can be lost in symptomatic SOD1G93A mice in contrast with age-matched controls. High levels of intra-terminal Ca^{2+} can lead to desensitization of intracellular Ca^{2+} release machinery such as RyR [134].The Ca^{2+} dysfunction in SOD1G93A animals could therefore impair the regulatory action of A2AR in the mobilization of internal Ca^{2+} stores. This could result in the observed unchanged MEPP and GMEPP frequency when CGS

21680 was added to the physiological solution in symptomatic SOD1G93A mice.

WT mice present an increase in MEPP frequency in 12-14 wo animals when compared to 4-6 wo mice in the presence of CGS 21680 (5nM). This could be a feature of NMJ maturation, like previously suggested when discussing the evoked activity. Symptomatic SOD1G93A NMT modulation of spontaneous activity is lost, highlighting neurodegenerative processes that impair both evoked and spontaneous ACh release in this rodent model of ALS.

6. Summary and Conclusions

We have put in evidence that pre-symptomatic SOD1G93A mice have a functional upregulation of A2AR in diaphragmatic NMJs, resulting in increased evoked quantal release when comparing to age-matched WT mice. Desynchronized (MEPPs) and synchronized (GMEPPs) spontaneous release frequency was also increased in SOD1G93A mice when A2AR were activated. This suggested the occurrence of changes in intraterminal [Ca^{2+}] regulation of ACh release in this mouse model involving A2AR signaling before symptoms onset.

The A2AR pre-symptomatic functional enhancement is lost when symptoms arise. This might be attributable to the pathological mechanisms inherent to the disease or to an adaptive shift in order to avoid intraterminal Ca^{2+} overload that would predispose MNs to cell death and increased functional impairment.

Our work points out changes related with A2AR role in the control of ACh release in SOD1G93A NMJs, highlighting the role of these purinergic receptors in disease progression and as a possible pharmacological target in ALS.

7. Future developments

The crosstalk between A1R and A2AR receptors must be explored in this model (work in progress). This may unveil different control and interaction between these receptors suggestible of the changes observed in the A2AR study.

Experiments with adenosine deaminase, may help to unveil if endogenous adenosine is masking the CGS 21680 effect in symptomatic animals either by desensitization of A2AR, tonic activation of A1R resulting in decreased A2AR function or increased binding competition with the A2AR agonist.

Due to the role of VGCC in ALS, more specifically the L-type, experiments with nitrendipine could be conducted in the presence of CGS 21680 to understand the role of A2AR in the recruitment of these channels. Blockers of P/Q-type and N-type VGCC could also be explored. The high affinity Ca^{2+} chelator BAPTA-AM could also be included in this role of experiments, together with the low affinity Ca^{2+} chelator EGTA-AM, in order to access the role and the tridimensional relationship between VGCC function and recruitment by A2AR in SOD1G93A. These two chelators could also be tested in the presence of ryanodine (RyR blocker) and tapsigargin (inhibitor of the sacro/endoplasmatic reticulum Ca^{2+} ATP-ase) to fully understand to role in intracellular store Ca^{2+} mobilization by A2AR in SOD1G93A mice.

It would also be interesting to explore if the A2AR changes in the NMJ of SOD1G93A are reverberated in the spinal cord and motor cortex, in order to

explore the pattern of adenosinergic dysfunction in ALS from the central nervous system to the most peripheral synapse.

8. Acknowledgements

Gostava de agradecer ao Professor Joaquim A. Ribeiro por me ter recebido no seu grupo de investigação e me ter orientado transmitindo sempre um entusiasmo científico contagiante e ensinado a ser rigoroso na minha prática científica.

À Professora Ana Sebastião por me ter acolhido no Instituto de Farmacologia e Neurociências e pela ajuda crucial na estruturação das minhas experiências e entendimento de resultados, sem a qual ficaria por vezes perdido.

À Alexandra Marçal por todo o apoio e motivação que foram fundamentais para eu conseguir prosseguir com o trabalho nos momentos mais difíceis. O rigor na análise e a organização são características que creio ter melhorado sob a sua orientação.

À Paula Pousinha pela disponibilidade e imensa simpatia na ajuda que dispôs.

Ao Rui Gomes por ter feito as genotipagens dos animais e pelo bom humor diário.

À Iolanda por cuidar dos animais, pela simpatia e disponibilidade imediata em resolver qualquer tipo de problemas.

À Mariana Rocha por me ter introduzido à técnica de electrofisiologia e ao Gonçalo Ramos, que inicialmente me ajudaram a integrar no grupo.

Aos meus colegas de laboratório sem os quais este trabalho não seria possível graças à sua sempre prestável ajuda e disponibilidade em me ajudar ora com problemas técnicos ora na aprendizagem de conceitos importantes no trabalho. O ambiente laboratorial criado por todos muito contribuiu para um bem-estar repleto de alegria que se prende numa amizade "científica" entre todos.

9. Bibliography

1. Goetz, C.G., *Amyotrophic lateral sclerosis: early contributions of Jean-Martin Charcot.* Muscle Nerve, 2000. **23**(3): p. 336-43.

2. Turner, M.R., O. Hardiman, M. Benatar, B.R. Brooks, A. Chio, M. de Carvalho, P.G. Ince, C. Lin, R.G. Miller, H. Mitsumoto, G. Nicholson, J. Ravits, P.J. Shaw, M. Swash, K. Talbot, B.J. Traynor, L.H. Van den Berg, J.H. Veldink, S. Vucic, and M.C. Kiernan, *Controversies and priorities in amyotrophic lateral sclerosis.* Lancet Neurol, 2013. **12**(3): p. 310-22.

3. Hardiman, O., L.H. van den Berg, and M.C. Kiernan, *Clinical diagnosis and management of amyotrophic lateral sclerosis.* Nat Rev Neurol, 2011. **7**(11): p. 639-49.

4. Turner, M.R., J. Scaber, J.A. Goodfellow, M.E. Lord, R. Marsden, and K. Talbot, *The diagnostic pathway and prognosis in bulbar-onset amyotrophic lateral sclerosis.* J Neurol Sci, 2010. **294**(1-2): p. 81-5.

5. Rosen, A.D., *Amyotrophic lateral sclerosis. Clinical features and prognosis.* Arch Neurol, 1978. **35**(10): p. 638-42.

6. Kiernan, M.C., S. Vucic, B.C. Cheah, M.R. Turner, A. Eisen, O. Hardiman, J.R. Burrell, and M.C. Zoing, *Amyotrophic lateral sclerosis.* Lancet, 2011. **377**(9769): p. 942-55.

7. Inghilleri, M. and E. Iacovelli, *Clinical neurophysiology in ALS.* Arch Ital Biol, 2011. **149**(1): p. 57-63.

8. de Carvalho, M. and M. Swash, *Fasciculation potentials: a study of amyotrophic lateral sclerosis and other neurogenic disorders.* Muscle Nerve, 1998. **21**(3): p. 336-44.

9. Vucic, S. and M.C. Kiernan, *Axonal excitability properties in amyotrophic lateral sclerosis.* Clin Neurophysiol, 2006. **117**(7): p. 1458-66.

10. Shefner, J.M., M.L. Watson, L. Simionescu, J.B. Caress, T.M. Burns, N.J. Maragakis, M. Benatar, W.S. David, K.R. Sharma, and S.B. Rutkove, *Multipoint incremental motor unit number estimation as an outcome measure in ALS.* Neurology, 2011. **77**(3): p. 235-41.

11. Olney, R.K. and C. Lomen-Hoerth, *Motor unit number estimation (MUNE): how may it contribute to the diagnosis of ALS?* Amyotroph Lateral Scler Other Motor Neuron Disord, 2000. **1 Suppl 2**: p. S41-4.

12. Singh, V., J. Gibson, B. McLean, M. Boggild, N. Silver, and R. White, *Fasciculations and cramps: how benign? Report of four cases progressing to ALS.* J Neurol, 2011. **258**(4): p. 573-8.

13. Wijesekera, L.C. and P.N. Leigh, *Amyotrophic lateral sclerosis.* Orphanet J Rare Dis, 2009. **4**: p. 3.

14. Byrne, S., M. Elamin, P. Bede, and O. Hardiman, *Absence of consensus in diagnostic criteria for familial neurodegenerative diseases.* J Neurol Neurosurg Psychiatry, 2012. **83**(4): p. 365-7.

15. *ALS ONLINE GENETICS DATABASE*. 2013 June 2013]; Available from: http://alsod.iop.kcl.ac.uk/.

16. McGoldrick, P., P.I. Joyce, E.M. Fisher, and L. Greensmith, *Rodent models of amyotrophic lateral sclerosis.* Biochim Biophys Acta, 2013.

17. Gurney, M.E., H. Pu, A.Y. Chiu, M.C. Dal Canto, C.Y. Polchow, D.D. Alexander, J. Caliendo, A. Hentati, Y.W. Kwon, H.X. Deng, and et al., *Motor neuron degeneration in mice that express a human Cu,Zn superoxide dismutase mutation.* Science, 1994. **264**(5166): p. 1772-5.

18. Maekawa, S., P.N. Leigh, A. King, E. Jones, J.C. Steele, I. Bodi, C.E. Shaw, T. Hortobagyi, and S. Al-Sarraj, *TDP-43 is consistently co-localized with ubiquitinated inclusions in sporadic and Guam amyotrophic lateral sclerosis but not in familial amyotrophic lateral sclerosis with and without SOD1 mutations.* Neuropathology, 2009. **29**(6): p. 672-83.

19. Sreedharan, J., I.P. Blair, V.B. Tripathi, X. Hu, C. Vance, B. Rogelj, S. Ackerley, J.C. Durnall, K.L. Williams, E. Buratti, F. Baralle, J. de Belleroche, J.D. Mitchell, P.N. Leigh, A. Al-Chalabi, C.C. Miller, G. Nicholson, and C.E. Shaw, *TDP-43 mutations in familial and sporadic amyotrophic lateral sclerosis.* Science, 2008. **319**(5870): p. 1668-72.

20. Verma, A. and R. Tandan, *RNA quality control and protein aggregates in amyotrophic lateral sclerosis: a review.* Muscle Nerve, 2013. **47**(3): p. 330-8.

21. Al-Chalabi, A., S. Kwak, M. Mehler, G. Rouleau, T. Siddique, M. Strong, and P.N. Leigh, *Genetic and epigenetic studies of amyotrophic lateral sclerosis.* Amyotroph Lateral Scler Frontotemporal Degener, 2013. **14 Suppl 1**: p. 44-52.

22. van Blitterswijk, M., M. DeJesus-Hernandez, and R. Rademakers, *How do C9ORF72 repeat expansions cause amyotrophic lateral sclerosis and frontotemporal dementia: can we learn from other noncoding repeat expansion disorders?* Curr Opin Neurol, 2012. **25**(6): p. 689-700.

23. Williams, K.L., J.A. Fifita, S. Vucic, J.C. Durnall, M.C. Kiernan, I.P. Blair, and G.A. Nicholson, *Pathophysiological insights into ALS with C9ORF72 expansions.* J Neurol Neurosurg Psychiatry, 2013.

24. Ciura, S., S. Lattante, I. Le Ber, M. Latouche, H. Tostivint, A. Brice, and E. Kabashi, *Loss of function of C9orf72 causes motor deficits in a zebrafish model of Amyotrophic Lateral Sclerosis.* Ann Neurol, 2013.

25. Robberecht, W. and T. Philips, *The changing scene of amyotrophic lateral sclerosis.* Nat Rev Neurosci, 2013. **14**(4): p. 248-64.

26. Kanning, K.C., A. Kaplan, and C.E. Henderson, *Motor neuron diversity in development and disease.* Annu Rev Neurosci, 2010. **33**: p. 409-40.

27. Benatar, M. and J. Wuu, *Presymptomatic studies in ALS: rationale, challenges, and approach.* Neurology, 2012. **79**(16): p. 1732-9.

28. Azzouz, M., N. Leclerc, M. Gurney, J.M. Warter, P. Poindron, and J. Borg, *Progressive motor neuron impairment in an animal model of familial amyotrophic lateral sclerosis.* Muscle Nerve, 1997. **20**(1): p. 45-51.

29. Pieri, M., I. Carunchio, L. Curcio, N.B. Mercuri, and C. Zona, *Increased persistent sodium current determines cortical hyperexcitability in a*

genetic model of amyotrophic lateral sclerosis. Exp Neurol, 2009. **215**(2): p. 368-79.

30. van Zundert, B., M.H. Peuscher, M. Hynynen, A. Chen, R.L. Neve, R.H. Brown, Jr., M. Constantine-Paton, and M.C. Bellingham, *Neonatal neuronal circuitry shows hyperexcitable disturbance in a mouse model of the adult-onset neurodegenerative disease amyotrophic lateral sclerosis.* J Neurosci, 2008. **28**(43): p. 10864-74.

31. Rocha, M. C., P. A. Pousinha, A. M. Correia, A. M. Sebastião and J. A. Ribeiro, *Early Changes of Neuromuscular Transmission in the SOD1(G93A) Mice Model of ALS Start Long before Motor Symptoms Onset.* PLoS One, 2013. **8**(9): e73846.

32. de Carvalho, M. and M. Swash, *The onset of ALS?* Clin Neurophysiol, 2010. **121**(10): p. 1709-10.

33. van Zundert, B., P. Izaurieta, E. Fritz, and F.J. Alvarez, *Early pathogenesis in the adult-onset neurodegenerative disease amyotrophic lateral sclerosis.* J Cell Biochem, 2012. **113**(11): p. 3301-12.

34. Vucic, S. and M.C. Kiernan, *Upregulation of persistent sodium conductances in familial ALS.* J Neurol Neurosurg Psychiatry, 2010. **81**(2): p. 222-7.

35. Wootz, H., E. Fitzsimons-Kantamneni, M. Larhammar, T.M. Rotterman, A. Enjin, K. Patra, E. Andre, B. Van Zundert, K. Kullander, and F.J. Alvarez, *Alterations in the motor neuron-renshaw cell circuit in the Sod1(G93A) mouse model.* J Comp Neurol, 2013. **521**(7): p. 1449-69.

36. Zhao, P., S. Ignacio, E.C. Beattie, and M.E. Abood, *Altered presymptomatic AMPA and cannabinoid receptor trafficking in motor neurons of ALS model mice: implications for excitotoxicity.* Eur J Neurosci, 2008. **27**(3): p. 572-9.

37. Fritz, E., P. Izaurieta, A. Weiss, F.R. Mir, P. Rojas, D. Gonzalez, F. Rojas, R.H. Brown, Jr., R. Madrid, and B. van Zundert, *Mutant SOD1-expressing astrocytes release toxic factors that trigger motoneuron death by inducing hyperexcitability.* J Neurophysiol, 2013. **109**(11): p. 2803-14.

38. Kanai, K., K. Shibuya, Y. Sato, S. Misawa, S. Nasu, Y. Sekiguchi, S. Mitsuma, S. Isose, Y. Fujimaki, S. Ohmori, S. Koga, and S. Kuwabara, *Motor axonal excitability properties are strong predictors for survival in amyotrophic lateral sclerosis.* J Neurol Neurosurg Psychiatry, 2012. **83**(7): p. 734-8.

39. Vucic, S., G.A. Nicholson, and M.C. Kiernan, *Cortical hyperexcitability may precede the onset of familial amyotrophic lateral sclerosis.* Brain, 2008. **131**(Pt 6): p. 1540-50.

40. Hegedus, J., C.T. Putman, and T. Gordon, *Time course of preferential motor unit loss in the SOD1 G93A mouse model of amyotrophic lateral sclerosis.* Neurobiol Dis, 2007. **28**(2): p. 154-64.

41. Fischer, L.R., D.G. Culver, P. Tennant, A.A. Davis, M. Wang, A. Castellano-Sanchez, J. Khan, M.A. Polak, and J.D. Glass, *Amyotrophic lateral sclerosis is a distal axonopathy: evidence in mice and man.* Exp Neurol, 2004. **185**(2): p. 232-40.

42. Browne, S.E., L. Yang, J.P. DiMauro, S.W. Fuller, S.C. Licata, and M.F. Beal, *Bioenergetic abnormalities in discrete cerebral motor pathways presage spinal cord pathology in the G93A SOD1 mouse model of ALS.* Neurobiol Dis, 2006. **22**(3): p. 599-610.

43. Guipponi, M., Q.X. Li, L. Hyde, T. Beissbarth, G.K. Smyth, C.L. Masters, and H.S. Scott, *SAGE analysis of genes differentially expressed in presymptomatic TgSOD1G93A transgenic mice identified cellular processes involved in early stage of ALS pathology.* J Mol Neurosci, 2010. **41**(1): p. 172-82.

44. Raoul, C., E. Buhler, C. Sadeghi, A. Jacquier, P. Aebischer, B. Pettmann, C.E. Henderson, and G. Haase, *Chronic activation in presymptomatic amyotrophic lateral sclerosis (ALS) mice of a feedback loop involving Fas, Daxx, and FasL.* Proc Natl Acad Sci U S A, 2006. **103**(15): p. 6007-12.

45. Verstraete, E., J.H. Veldink, L.H. van den Berg, and M.P. van den Heuvel, *Structural brain network imaging shows expanding disconnection of the motor system in amyotrophic lateral sclerosis.* Hum Brain Mapp, 2013.

46. Hatazawa, J., R.A. Brooks, M.C. Dalakas, L. Mansi, and G. Di Chiro, *Cortical motor-sensory hypometabolism in amyotrophic lateral sclerosis: a PET study.* J Comput Assist Tomogr, 1988. **12**(4): p. 630-6.

47. Senda, J., S. Kato, T. Kaga, M. Ito, N. Atsuta, T. Nakamura, H. Watanabe, F. Tanaka, S. Naganawa, and G. Sobue, *Progressive and*

widespread brain damage in ALS: MRI voxel-based morphometry and diffusion tensor imaging study. Amyotroph Lateral Scler, 2011. **12**(1): p. 59-69.

48. Zang, D.W., Q. Yang, H.X. Wang, G. Egan, E.C. Lopes, and S.S. Cheema, *Magnetic resonance imaging reveals neuronal degeneration in the brainstem of the superoxide dismutase 1 transgenic mouse model of amyotrophic lateral sclerosis.* Eur J Neurosci, 2004. **20**(7): p. 1745-51.

49. Kang, S.H., Y. Li, M. Fukaya, I. Lorenzini, D.W. Cleveland, L.W. Ostrow, J.D. Rothstein, and D.E. Bergles, *Degeneration and impaired regeneration of gray matter oligodendrocytes in amyotrophic lateral sclerosis.* Nat Neurosci, 2013. **16**(5): p. 571-9.

50. Dupuis, L., H. Oudart, F. Rene, J.L. Gonzalez de Aguilar, and J.P. Loeffler, *Evidence for defective energy homeostasis in amyotrophic lateral sclerosis: benefit of a high-energy diet in a transgenic mouse model.* Proc Natl Acad Sci U S A, 2004. **101**(30): p. 11159-64.

51. Vaisman, N., M. Lusaus, B. Nefussy, E. Niv, D. Comaneshter, R. Hallack, and V.E. Drory, *Do patients with amyotrophic lateral sclerosis (ALS) have increased energy needs?* J Neurol Sci, 2009. **279**(1-2): p. 26-9.

52. Mancuso, R., S. Olivan, R. Osta, and X. Navarro, *Evolution of gait abnormalities in SOD1(G93A) transgenic mice.* Brain Res, 2011. **1406**: p. 65-73.

53. Loizzo, S., M. Pieri, A. Ferri, M.T. Carri, C. Zona, A. Fortuna, and S. Vella, *Dynamic NAD(P)H post-synaptic autofluorescence signals for the assessment of mitochondrial function in a neurodegenerative disease: monitoring the primary motor cortex of G93A mice, an amyotrophic lateral sclerosis model.* Mitochondrion, 2010. **10**(2): p. 108-14.

54. Casas, C., M. Herrando-Grabulosa, R. Manzano, R. Mancuso, R. Osta, and X. Navarro, *Early presymptomatic cholinergic dysfunction in a murine model of amyotrophic lateral sclerosis.* Brain Behav, 2013. **3**(2): p. 145-58.

55. Gerber, Y.N., J.C. Sabourin, M. Rabano, M. Vivanco, and F.E. Perrin, *Early functional deficit and microglial disturbances in a mouse model of amyotrophic lateral sclerosis.* PLoS One, 2012. **7**(4): p. e36000.

56. Zona, C., M. Pieri, and I. Carunchio, *Voltage-dependent sodium channels in spinal cord motor neurons display rapid recovery from fast inactivation in a mouse model of amyotrophic lateral sclerosis.* J Neurophysiol, 2006. **96**(6): p. 3314-22.

57. Cheroni, C., M. Peviani, P. Cascio, S. Debiasi, C. Monti, and C. Bendotti, *Accumulation of human SOD1 and ubiquitinated deposits in the spinal cord of SOD1G93A mice during motor neuron disease progression correlates with a decrease of proteasome.* Neurobiol Dis, 2005. **18**(3): p. 509-22.

58. Zhao, W., D.R. Beers, J.S. Henkel, W. Zhang, M. Urushitani, J.P. Julien, and S.H. Appel, *Extracellular mutant SOD1 induces microglial-mediated motoneuron injury.* Glia, 2010. **58**(2): p. 231-43.

59. Grosskreutz, J., L. Van Den Bosch, and B.U. Keller, *Calcium dysregulation in amyotrophic lateral sclerosis.* Cell Calcium, 2010. **47**(2): p. 165-74.

60. Pardo, A.C., V. Wong, L.M. Benson, M. Dykes, K. Tanaka, J.D. Rothstein, and N.J. Maragakis, *Loss of the astrocyte glutamate transporter GLT1 modifies disease in SOD1(G93A) mice.* Exp Neurol, 2006. **201**(1): p. 120-30.

61. Bilsland, L.G., E. Sahai, G. Kelly, M. Golding, L. Greensmith, and G. Schiavo, *Deficits in axonal transport precede ALS symptoms in vivo.* Proc Natl Acad Sci U S A, 2010. **107**(47): p. 20523-8.

62. Marcuzzo, S., I. Zucca, A. Mastropietro, N.K. de Rosbo, P. Cavalcante, S. Tartari, S. Bonanno, L. Preite, R. Mantegazza, and P. Bernasconi, *Hind limb muscle atrophy precedes cerebral neuronal degeneration in G93A-SOD1 mouse model of amyotrophic lateral sclerosis: a longitudinal MRI study.* Exp Neurol, 2011. **231**(1): p. 30-7.

63. Fuchs, A., S. Kutterer, T. Muhling, J. Duda, B. Schutz, B. Liss, B.U. Keller, and J. Roeper, *Selective mitochondrial Ca2+ uptake deficit in disease endstage vulnerable motoneurons of the SOD1G93A mouse model of amyotrophic lateral sclerosis.* J Physiol, 2013. **591**(Pt 10): p. 2723-45.

64. Fergani, A., H. Oudart, J.L. Gonzalez De Aguilar, B. Fricker, F. Rene, J.F. Hocquette, V. Meininger, L. Dupuis, and J.P. Loeffler, *Increased peripheral lipid clearance in an animal model of amyotrophic lateral sclerosis.* J Lipid Res, 2007. **48**(7): p. 1571-80.

65. Wong, F., L. Fan, S. Wells, R. Hartley, F.E. Mackenzie, O. Oyebode, R. Brown, D. Thomson, M.P. Coleman, G. Blanco, and R.R. Ribchester, *Axonal and neuromuscular synaptic phenotypes in Wld(S), SOD1(G93A) and ostes mutant mice identified by fiber-optic confocal microendoscopy.* Mol Cell Neurosci, 2009. **42**(4): p. 296-307.

66. Bjornskov, E.K., F.H. Norris, Jr., and J. Mower-Kuby, *Quantitative axon terminal and end-plate morphology in amyotrophic lateral sclerosis.* Arch Neurol, 1984. **41**(5): p. 527-30.

67. Appel, S.H., J.I. Engelhardt, J. Garcia, and E. Stefani, *Immunoglobulins from animal models of motor neuron disease and from human amyotrophic lateral sclerosis patients passively transfer physiological abnormalities to the neuromuscular junction.* Proc Natl Acad Sci U S A, 1991. **88**(2): p. 647-51.

68. O'Shaughnessy, T.J., H. Yan, J. Kim, E.H. Middlekauff, K.W. Lee, L.H. Phillips, and Y.I. Kim, *Amyotrophic lateral sclerosis: serum factors enhance spontaneous and evoked transmitter release at the neuromuscular junction.* Muscle Nerve, 1998. **21**(1): p. 81-90.

69. Krakora, D., C. Macrander, and M. Suzuki, *Neuromuscular junction protection for the potential treatment of amyotrophic lateral sclerosis.* Neurol Res Int, 2012. **2012**: p. 379657.

70. Naumenko, N., E. Pollari, A. Kurronen, R. Giniatullina, A. Shakirzyanova, J. Magga, J. Koistinaho, and R. Giniatullin, *Gender-Specific Mechanism of Synaptic Impairment and Its Prevention by GCSF in a Mouse Model of ALS.* Front Cell Neurosci, 2011. **5**: p. 26.

71. Souayah, N., K.M. Coakley, R. Chen, N. Ende, and J.J. McArdle, *Defective neuromuscular transmission in the SOD1 G93A transgenic mouse improves after administration of human umbilical cord blood cells.* Stem Cell Rev, 2012. **8**(1): p. 224-8.

72. Martyn, J.A., M.J. Fagerlund, and L.I. Eriksson, *Basic principles of neuromuscular transmission.* Anaesthesia, 2009. **64 Suppl 1**: p. 1-9.

73. Ribeiro, J.A., R.A. Cunha, P. Correia-de-Sá, and A.M. Sebastião, *Purinergic regulation of acetylcholine release.* Prog Brain Res, 1996. **109**: p. 231-41.

74. Ruff, R.L., *Endplate contributions to the safety factor for neuromuscular transmission.* Muscle Nerve, 2011. **44**(6): p. 854-61.

75. Wood, S.J. and C.R. Slater, *Safety factor at the neuromuscular junction.* Prog Neurobiol, 2001. **64**(4): p. 393-429.

76. Telerman-Toppet, N. and C. Coers, *Motor innervation and fiber type pattern in amyotrophic lateral sclerosis and in Charcot-Marie-Tooth disease.* Muscle Nerve, 1978. **1**(2): p. 133-9.

77. Pinelli, P., F. Pisano, F. Ceriani, and G. Miscio, *EMG evaluation of motor neuron sprouting in amyotrophic lateral sclerosis.* Ital J Neurol Sci, 1991. **12**(4): p. 359-67.

78. Van der Neut, R., W.H. Gispen, and P.R. Bar, *Serum from patients with amyotrophic lateral sclerosis induces the expression of B-50/GAP-43 and neurofilament in cultured rat fetal spinal neurons.* Mol Chem Neuropathol, 1991. **14**(3): p. 247-58.

79. Krivickas, L.S., J.I. Yang, S.K. Kim, and W.R. Frontera, *Skeletal muscle fiber function and rate of disease progression in amyotrophic lateral sclerosis.* Muscle Nerve, 2002. **26**(5): p. 636-43.

80. Frey, D., C. Schneider, L. Xu, J. Borg, W. Spooren, and P. Caroni, *Early and selective loss of neuromuscular synapse subtypes with low sprouting competence in motoneuron diseases.* J Neurosci, 2000. **20**(7): p. 2534-42.

81. Narai, H., Y. Manabe, M. Nagai, I. Nagano, Y. Ohta, T. Murakami, Y. Takehisa, T. Kamiya, and K. Abe, *Early detachment of neuromuscular junction proteins in ALS mice with SODG93A mutation.* Neurol Int, 2009. **1**(1): p. e16.

82. Dadon-Nachum, M., E. Melamed, and D. Offen, *The "dying-back" phenomenon of motor neurons in ALS.* J Mol Neurosci, 2011. **43**(3): p. 470-7.

83. Dupuis, L. and J.P. Loeffler, *Neuromuscular junction destruction during amyotrophic lateral sclerosis: insights from transgenic models.* Curr Opin Pharmacol, 2009. **9**(3): p. 341-6.

84. Uchitel, O.D., F. Scornik, D.A. Protti, C.G. Fumberg, V. Alvarez, and S.H. Appel, *Long-term neuromuscular dysfunction produced by passive transfer of amyotrophic lateral sclerosis immunoglobulins.* Neurology, 1992. **42**(11): p. 2175-80.

85. Uchitel, O.D., S.H. Appel, F. Crawford, and L. Sczcupak, *Immunoglobulins from amyotrophic lateral sclerosis patients enhance spontaneous transmitter release from motor-nerve terminals.* Proc Natl Acad Sci U S A, 1988. **85**(19): p. 7371-4.

86. Kim, Y. I., C. Joo, C. C. Cheng, C. E. Davis and T. J. O'Shaughnessy, *Neuromuscular transmission in a transgenic animal model of motor neuron disease*. Proceedings of the 18th Annual International Conference of the Ieee Engineering in Medicine and Biology Society, 1997. Vol 18, Pts 1-5 18: 1773-1774.

87. Fratantoni, S.A., A.L. Dubrovsky, and O.D. Uchitel, *Uptake of immunoglobulin G from amyotrophic lateral sclerosis patients by motor nerve terminals in mice.* J Neurol Sci, 1996. **137**(2): p. 97-102.

88. Fratantoni, S.A., G. Weisz, A.M. Pardal, R.C. Reisin, and O.D. Uchitel, *Amyotrophic lateral sclerosis IgG-treated neuromuscular junctions develop sensitivity to L-type calcium channel blocker.* Muscle Nerve, 2000. **23**(4): p. 543-50.

89. Correia-de-Sá, P., M.A. Timóteo, and J.A. Ribeiro, *Influence of stimulation on Ca(2+) recruitment triggering [3H]acetylcholine release from the rat motor-nerve endings.* Eur J Pharmacol, 2000. **406**(3): p. 355-62.

90. Robitaille, R., E.M. Adler, and M.P. Charlton, *Strategic location of calcium channels at transmitter release sites of frog neuromuscular synapses.* Neuron, 1990. **5**(6): p. 773-9.

91. Oliveira, L., M.A. Timóteo, and P. Correia-de-Sá, *Tetanic depression is overcome by tonic adenosine A(2A) receptor facilitation of L-type Ca(2+) influx into rat motor nerve terminals.* J Physiol, 2004. **560**(Pt 1): p. 157-68.

92. Miller, R.G., J.D. Mitchell, and D.H. Moore, *Riluzole for amyotrophic lateral sclerosis (ALS)/motor neuron disease (MND).* Cochrane Database Syst Rev, 2012. **3**: p. CD001447.

93. Sebastião, A.M. and J.A. Ribeiro, *Adenosine receptors and the central nervous system.* Handb Exp Pharmacol, 2009(193): p. 471-534.

94. Oliveira, L. and P. Correia-de-Sá, *Protein kinase A and Ca(v)1 (L-Type) channels are common targets to facilitatory adenosine A2A and*

muscarinic M1 receptors on rat motoneurons. Neurosignals, 2005. **14**(5): p. 262-72.

95. Sebastião, A.M. and J.A. Ribeiro, *Fine-tuning neuromodulation by adenosine.* Trends Pharmacol Sci, 2000. **21**(9): p. 341-6.

96. Pousinha, P.A., A.M. Correia, A.M. Sebastião, and J.A. Ribeiro, *Predominance of adenosine excitatory over inhibitory effects on transmission at the neuromuscular junction of infant rats.* J Pharmacol Exp Ther, 2010. **332**(1): p. 153-63.

97. Correia-de-Sá, P., A.M. Sebastião, and J.A. Ribeiro, *Inhibitory and excitatory effects of adenosine receptor agonists on evoked transmitter release from phrenic nerve ending of the rat.* Br J Pharmacol, 1991. **103**(2): p. 1614-20.

98. Correia-de-Sá, P., M.A. Timóteo, and J.A. Ribeiro, *A(2A) adenosine receptor facilitation of neuromuscular transmission: influence of stimulus paradigm on calcium mobilization.* J Neurochem, 2000. **74**(6): p. 2462-9.

99. Pousinha, P.A., A.M. Correia, A.M. Sebastião, and J.A. Ribeiro, *Neuromuscular transmission modulation by adenosine upon aging.* Neurobiol Aging, 2012. **33**(12): p. 2869-80.

100. Pousinha, P.A., M.J. Diógenes, J.A. Ribeiro, and A.M. Sebastião, *Triggering of BDNF facilitatory action on neuromuscular transmission by adenosine A2A receptors.* Neurosci Lett, 2006. **404**(1-2): p. 143-7.

101. Pagani, M.R., R.C. Reisin, and O.D. Uchitel, *Calcium signaling pathways mediating synaptic potentiation triggered by amyotrophic lateral sclerosis IgG in motor nerve terminals.* J Neurosci, 2006. **26**(10): p. 2661-72.

102. Palma, A.G., S. Muchnik, and A.S. Losavio, *Excitatory effect of the A2A adenosine receptor agonist CGS-21680 on spontaneous and K+-evoked acetylcholine release at the mouse neuromuscular junction.* Neuroscience, 2011. **172**: p. 164-76.

103. Yanpallewar, S.U., C.A. Barrick, H. Buckley, J. Becker, and L. Tessarollo, *Deletion of the BDNF truncated receptor TrkB.T1 delays disease onset in a mouse model of amyotrophic lateral sclerosis.* PLoS One, 2012. **7**(6): p. e39946.

104. Potenza, R.L., M. Armida, A. Ferrante, A. Pezzola, A. Matteucci, M. Puopolo, and P. Popoli, *Effects of chronic caffeine intake in a mouse model of amyotrophic lateral sclerosis.* J Neurosci Res, 2013. **91**(4): p. 585-92.

105. Lopes, L.V., A.M. Sebastião, and J.A. Ribeiro, *Adenosine and related drugs in brain diseases: present and future in clinical trials.* Curr Top Med Chem, 2011. **11**(8): p. 1087-101.

106. Sebastião, A.M. and J.A. Ribeiro, *Triggering neurotrophic factor actions through adenosine A2A receptor activation: implications for neuroprotection.* Br J Pharmacol, 2009. **158**(1): p. 15-22.

107. Turner, B.J. and K. Talbot, *Transgenics, toxicity and therapeutics in rodent models of mutant SOD1-mediated familial ALS.* Prog Neurobiol, 2008. **85**(1): p. 94-134.

108. Krebs, H.A. and K. Henseleit, *Untersuchungen uber die Harnstoffbildung im Tierkoper.* Hoppe-Seyler's Z Physiol Chem 1932. **210**: p. 33-37.

109. Turkanis, S.A., *Effects of muscle stretch on transmitter release at end-plates of rat diaphragm and frog sartorius muscle.* J Physiol, 1973. **230**(2): p. 391-403.

110. Kamenskaya, M.A., D. Elmqvist, and S. Thesleff, *Guanidine and neuromuscular transmission. II. Effect on transmitter release in response to repetitive nerve stimulation.* Arch Neurol, 1975. **32**(8): p. 510-8.

111. Wessler, I., J. Rasbach, B. Scheuer, U. Hillen, and H. Kilbinger, *Effects of (+)-tubocurarine on [3H]acetylcholine release from the rat phrenic nerve at different stimulation frequencies and train lengths.* Naunyn Schmiedebergs Arch Pharmacol, 1987. **335**(5): p. 496-501.

112. Fatt, P. and B. Katz, *An analysis of the end-plate potential recorded with an intracellular electrode.* J Physiol, 1951. **115**(3): p. 320-70.

113. Bowman, W.C., *Neuromuscular block.* Br J Pharmacol, 2006. **147 Suppl 1**: p. S277-86.

114. Jenkinson, D.H., *The nature of the antagonism between calcium and magnesium ions at the neuromuscular junction.* J Physiol, 1957. **138**(3): p. 434-44.

115. Cruz, L.J., W.R. Gray, B.M. Olivera, R.D. Zeikus, L. Kerr, D. Yoshikami, and E. Moczydlowski, *Conus geographus toxins that discriminate between neuronal and muscle sodium channels.* J Biol Chem, 1985. **260**(16): p. 9280-8.

116. Neher, E., *Vesicle pools and Ca2+ microdomains: new tools for understanding their roles in neurotransmitter release.* Neuron, 1998. **20**(3): p. 389-99.

117. Martin, A.R., *A further study of the statistical composition on the end-plate potential.* J Physiol, 1955. **130**(1): p. 114-22.

118. Piriz, J., M.D. Rosato Siri, R. Pagani, and O.D. Uchitel, *Nifedipine-mediated mobilization of intracellular calcium stores increases spontaneous neurotransmitter release at neonatal rat motor nerve terminals.* J Pharmacol Exp Ther, 2003. **306**(2): p. 658-63.

119. Sellin, L.C., J. Molgo, K. Tornquist, B. Hansson, and S. Thesleff, *On the possible origin of giant or slow-rising miniature end-plate potentials at the neuromuscular junction.* Pflugers Arch, 1996. **431**(3): p. 325-34.

120. Di, L. and E.H. Kerns, *Biological assay challenges from compound solubility: strategies for bioassay optimization.* Drug Discov Today, 2006. **11**(9-10): p. 446-51.

121. Jarvis, M.F., R. Schulz, A.J. Hutchison, U.H. Do, M.A. Sills, and M. Williams, *[3H]CGS 21680, a selective A2 adenosine receptor agonist directly labels A2 receptors in rat brain.* J Pharmacol Exp Ther, 1989. **251**(3): p. 888-93.

122. Fredholm, B.B., K. Lindstrom, S. Dionisotti, and E. Ongini, *[3H]SCH 58261, a selective adenosine A2A receptor antagonist, is a useful ligand in autoradiographic studies.* J Neurochem, 1998. **70**(3): p. 1210-6.

123. Cunha, R.A. and A.M. Sebastião, *Extracellular metabolism of adenine nucleotides and adenosine in the innervated skeletal muscle of the frog.* Eur J Pharmacol, 1991. **197**(1): p. 83-92.

124. Sieck, D.C., W.Z. Zhan, Y.H. Fang, L.G. Ermilov, G.C. Sieck, and C.B. Mantilla, *Structure-activity relationships in rodent diaphragm muscle fibers vs. neuromuscular junctions.* Respir Physiol Neurobiol, 2012. **180**(1): p. 88-96.

125. Hegedus, J., C.T. Putman, and T. Gordon, *Progressive motor unit loss in the G93A mouse model of amyotrophic lateral sclerosis is unaffected by gender.* Muscle Nerve, 2009. **39**(3): p. 318-27.

126. Tsentsevitsky, A., I. Kovyazina, E. Nikolsky, E. Bukharaeva, and R. Giniatullin, *Redox Sensitive Synchronizing Action of Adenosine On Transmitter Release at the Neuromuscular Junction.* Neuroscience, 2013.

127. Komaki, S., K. Ishikawa, and Y. Arakawa, *Trk and cAMP-dependent survival activity of adenosine A(2A) agonist CGS21680 on rat motoneurons in culture.* Neurosci Lett, 2012. **522**(1): p. 21-4.

128. Catterall, W.A. and A.P. Few, *Calcium channel regulation and presynaptic plasticity.* Neuron, 2008. **59**(6): p. 882-901.

129. Pieri, M., S. Caioli, N. Canu, N.B. Mercuri, E. Guatteo, and C. Zona, *Over-expression of N-type calcium channels in cortical neurons from a mouse model of Amyotrophic Lateral Sclerosis.* Exp Neurol, 2012.

130. Muchnik, S., A. Losavio, and S. De Lorenzo, *Effect of amyotrophic lateral sclerosis serum on calcium channels related to spontaneous acetylcholine release.* Clin Neurophysiol, 2002. **113**(7): p. 1066-71.

131. Gonzalez, L.E., M.L. Kotler, L.G. Vattino, E. Conti, R.C. Reisin, K.J. Mulatz, T.P. Snutch, and O.D. Uchitel, *Amyotrophic lateral sclerosis-immunoglobulins selectively interact with neuromuscular junctions expressing P/Q-type calcium channels.* J Neurochem, 2011. **119**(4): p. 826-38.

132. Carter, J.R. and M. Mynlieff, *Amyotrophic lateral sclerosis patient IgG alters voltage dependence of Ca2+ channels in dissociated rat motoneurons.* Neurosci Lett, 2003. **353**(3): p. 221-5.

133. Ji, F., J. Han, B. Liu, H. Wang, G. Shen, and J. Tao, *Vecuronium suppresses transmission at the rat phrenic neuromuscular junction by inhibiting presynaptic L-type calcium channels.* Neurosci Lett, 2013. **533**: p. 1-6.

134. Morrissette, J., L. Xu, A. Nelson, G. Meissner, and B.A. Block, *Characterization of RyR1-slow, a ryanodine receptor specific to slow-twitch skeletal muscle.* Am J Physiol Regul Integr Comp Physiol, 2000. **279**(5): p. R1889-98.

135. Endo, M., *Calcium-induced calcium release in skeletal muscle.* Physiol Rev, 2009. **89**(4): p. 1153-76.

136. Norris, F.H., Jr. and E.L. Gasteiger, *Action potentials of single motor units in normal muscle.* Electroencephalogr Clin Neurophysiol, 1955. **7**(1): p. 115-25.

137. Urbano, F.J., R.S. Depetris, and O.D. Uchitel, *Coupling of L-type calcium channels to neurotransmitter release at mouse motor nerve terminals.* Pflugers Arch, 2001. **441**(6): p. 824-31.

138. Alexianu, M.E., M. Kozovska, and S.H. Appel, *Immune reactivity in a mouse model of familial ALS correlates with disease progression.* Neurology, 2001. **57**(7): p. 1282-9.

139. Weinstein, S.P., *A comparative electrophysiological study of motor end-plate diseased skeletal muscle in the mouse.* J Physiol, 1980. **307**: p. 453-64.

140. Kim, Y.I., T. Lomo, M.T. Lupa, and S. Thesleff, *Miniature end-plate potentials in rat skeletal muscle poisoned with botulinum toxin.* J Physiol, 1984. **356**: p. 587-99.

141. Vautrin, J. and M.E. Kriebel, *Giant and sub-miniature end-plate potentials.* Pflugers Arch, 1997. **433**(5): p. 669-70.

142. Timóteo, M.A., M. Faria, and P. Correia-de-Sá, *Endogenous adenosine prevents post-tetanic release facilitation mediated by alpha3beta2 nicotinic autoreceptors.* Eur J Pharmacol, 2003. **464**(2-3): p. 115-25.

143. Noronha-Matos, J.B., T. Morais, D. Trigo, M.A. Timóteo, M.T. Magalhaes-Cardoso, L. Oliveira, and P. Correia-de-Sá, *Tetanic failure due to decreased endogenous adenosine A(2A) tonus operating neuronal Ca(v) 1 (L-type) influx in Myasthenia gravis.* J Neurochem, 2011. **117**(5): p. 797-811.

144. Kovalevskaya, N.V., M. van de Waterbeemd, F.M. Bokhovchuk, N. Bate, R.J. Bindels, J.G. Hoenderop, and G.W. Vuister, *Structural analysis of calmodulin binding to ion channels demonstrates the role of its plasticity in regulation.* Pflugers Arch, 2013.

145. Navarro, G., M.S. Aymerich, D. Marcellino, A. Cortes, V. Casado, J. Mallol, E.I. Canela, L. Agnati, A.S. Woods, K. Fuxe, C. Lluis, J.L. Lanciego, S. Ferre, and R. Franco, *Interactions between calmodulin, adenosine A2A, and dopamine D2 receptors.* J Biol Chem, 2009. **284**(41): p. 28058-68.

146. Lynge, J., C. Juel, and Y. Hellsten, *Extracellular formation and uptake of adenosine during skeletal muscle contraction in the rat: role of adenosine transporters.* J Physiol, 2001. **537**(Pt 2): p. 597-605.

147. Valdez, G., J.C. Tapia, J.W. Lichtman, M.A. Fox, and J.R. Sanes, *Shared resistance to aging and ALS in neuromuscular junctions of specific muscles.* PLoS One, 2012. **7**(4): p. e34640.

148. Chai, R.J., J. Vukovic, S. Dunlop, M.D. Grounds, and T. Shavlakadze, *Striking denervation of neuromuscular junctions without lumbar*

motoneuron loss in geriatric mouse muscle. PLoS One, 2011. **6**(12): p. e28090.

149. Deschenes, M.R., M.A. Roby, and E.K. Glass, *Aging influences adaptations of the neuromuscular junction to endurance training.* Neuroscience, 2011. **190**: p. 56-66.

150. Jorquera, G., F. Altamirano, A. Contreras-Ferrat, G. Almarza, S. Buvinic, V. Jacquemond, E. Jaimovich, and M. Casas, *Cav1.1 controls frequency-dependent events regulating adult skeletal muscle plasticity.* J Cell Sci, 2013. **126**(Pt 5): p. 1189-98.

151. Parakh, S., D.M. Spencer, M.A. Halloran, K.Y. Soo, and J.D. Atkin, *Redox regulation in amyotrophic lateral sclerosis.* Oxid Med Cell Longev, 2013. **2013**: p. 408681.